AN EXPERIMENTAL INVESTIGATION OF THERMOACOUSTIC LASERS OPERATING IN AUDIBLE FREQUENCY RANGE

by

Sanket Anil Kolhe

A thesis submitted to the faculty of
The University of Utah
in partial fulfillment of the requirements for the degree of

Master of Science

Department of Mechanical Engineering

The University of Utah

December 2012

The University of Utah Graduate School

STATEMENT OF THESIS APPROVAL

The thesis of **Sanket Anil Kolhe**

has been approved by the following supervisory committee members:

Kuan Chen	, Chair	**01/04/2012** Date Approved
Timothy Ameel	, Member	**01/04/2012** Date Approved
Kent Udell	, Member	**01/04/2012** Date Approved

and by **Timothy Ameel** , Chair of the Department of **Mechanical Engineering**

and by Charles A. Wight, Dean of The Graduate School.

ABSTRACT

Thermoacoustic lasers convert heat from a high-temperature heat source into acoustic power while rejecting waste heat to a low temperature sink. The working fluids involved can be air or noble gases which are nontoxic and environmentally benign. Simple in construction due to absence of moving parts, thermoacoustic lasers can be employed to achieve generation of electricity at individual homes, water-heating for domestic purposes, and to facilitate space heating and cooling. The possibility of utilizing waste heat or solar energy to run thermoacoustic devices makes them technically promising and economically viable to generate large quantities of acoustic energy.

The research presented in this thesis deals with the effects of geometric parameters (stack position, stack length, tube length) associated with a thermoacoustic laser on the output sound wave. The effects of varying input power on acoustic output were also studied. Based on the experiments, optimum operating conditions were identified and qualitative and/or quantitative explanations were provided to justify our observations. It was observed that the maximum sound pressure level was generated for the laser with the stack positioned at a distance of quarter lengths of a resonator from the closed end. Higher sound pressure levels were recorded for the laser with longer stack lengths and longer resonator lengths. Efforts were also made to develop high-frequency thermoacoustic lasers.

TABLE OF CONTENTS

LIST OF FIGURES

LIST OF TABLES

CHAPTER 1

INTRODUCTION

1.1 Introduction to Thermodynamic Cycles

Thermodynamics studies have taught us that there are two important areas of application for thermodynamics: power generation and refrigeration. Power generation is accomplished by prime movers or engines and they operate on thermodynamic cycles called power cycles. On the other hand, refrigeration is accomplished by refrigerators, air conditioners, or heat pumps and they operate on refrigeration cycles. In a prime mover, heat flows through the system from high to low temperature and work is generated, as shown in Figure 1.1, while in a heat pump, the flows of heat and work are reversed, i.e., work is absorbed by the system to pump the heat from low temperature to high temperature.

Let T_H and T_L be the temperatures of the heat source and heat sink of a power cycle, respectively, Q_H and Q_C the associated heat flows, and W the work flow. Q_H, Q_C, and W are time-averaged entities. Assuming a steady flow, the first law of thermodynamics states that:

$$Q_H - Q_C - W = 0 \qquad (1.1)$$

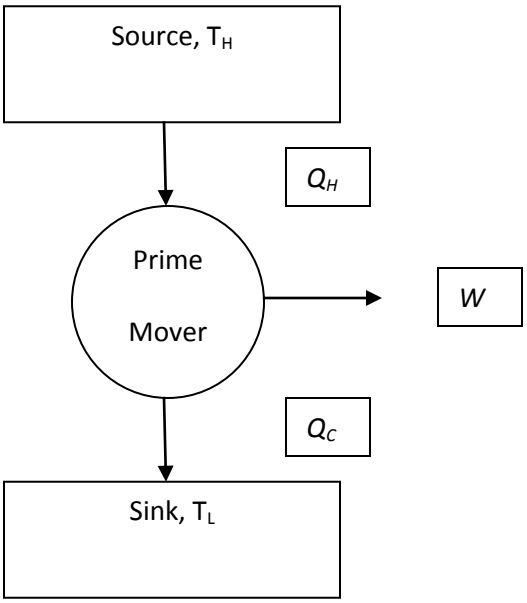

Figure 1.1: Prime mover

The right-hand side of equation (1.4) is called Carnot's efficiency η_C and it is the highest efficiency a prime mover can achieve. For a heat pump, the performance is expressed in terms of coefficient of performance COP = Q_C/W. Combining equations (1.1) and (1.3), we get:

$$\mathrm{COP} \leq T_C/(T_H - T_C) \qquad (1.2)$$

Once again, the right-hand side of equation (1.5) is called Carnot's coefficient of performance, COP_C.

An actual power cycle, however, differs from an ideal one mostly due to the irreversibilities associated with the system. Two common sources of irreversibilities are fluid friction and heat transfer across the finite temperature difference. The desire to approach Carnot's efficiency competes against the need for low cost, high reliability,

compactness, etc. The prime movers that are the subject of this literature are reasonably efficient and extremely simple.

1.2 Introduction to Thermoacoustic Prime Movers

Thermoacoustic Prime Movers are mechanically simple in construction and do not require moving parts, close tolerances, exotic materials, pistons, or valves. Thermoacoustic Prime Movers convert heat energy to sound energy. The prime mover under discussion is as shown in Figure 1.2. Basic components of this prime mover include a resonator, a stack, and two heat exchangers across the stack. A resonator is a glass tube with one end closed and the other end open to air. The stack used in the prime mover under discussion is a plug of ceramic automotive catalytic converter. The hot heat exchanger is made of Nichrome heater wire wound around the grooves at one end of the ceramic plug. There is no need for a cold heat exchanger for the prime mover under study, since the other end of the stack faces the open end of the glass tube. Cooling takes place in such prime movers due to natural convection and radiation. Electric current passing through the heater wire at one end creates a temperature gradient across the stack, and when this temperature difference crosses the critical temperature difference, the air in the glass tube oscillates to produce acoustic output. The sound wave generated has a pressure antinode at the closed end and a velocity antinode at the open end. Thus, a Thermoacoustic Prime Mover produces acoustic work by accepting heat input from a high-temperature heat source and by rejecting heat to the low-temperature heat sink.

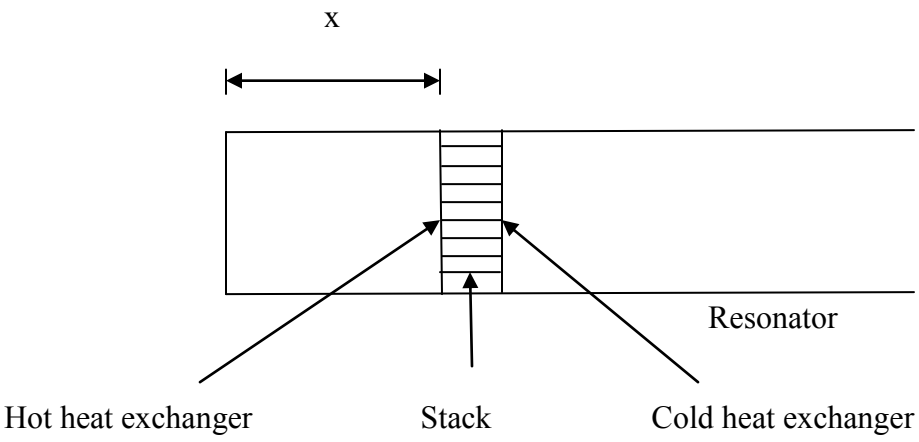

Figure 1.2: Thermoacoustic Prime Mover

1.3 Principle of Thermoacoustic Prime Movers

To understand the basic principle of the working of the Thermoacoustic Prime Mover, we will discuss G.W. Swift's (1988) explanation of the Thermoacoustic phenomenon from a Lagrangian point of view of fluid mechanics. We will consider a parcel of fluid and follow its movement. Figure 1.3 displays a cycle of a Thermoacoustic Prime Mover which is identical to the Brayton cycle. For simplicity of understanding, the sound wave is considered to be a square wave instead of a sinusoidal wave, due to which our thermodynamic cycles appears to have two reversible adiabatic processes and two irreversible isobaric processes.

In a traditional heat engine, valves and pistons move with a correct timing for the operation of the engine. Although a Thermoacoustic laser does not contain any such moving parts, a similar phasing is seen due to the presence of two thermodynamic media: fluid in the converter and solid plates of the porous stack plug. When the fluid oscillates in the convertor with acoustic frequency, the temperature of the fluid undergoes a change.

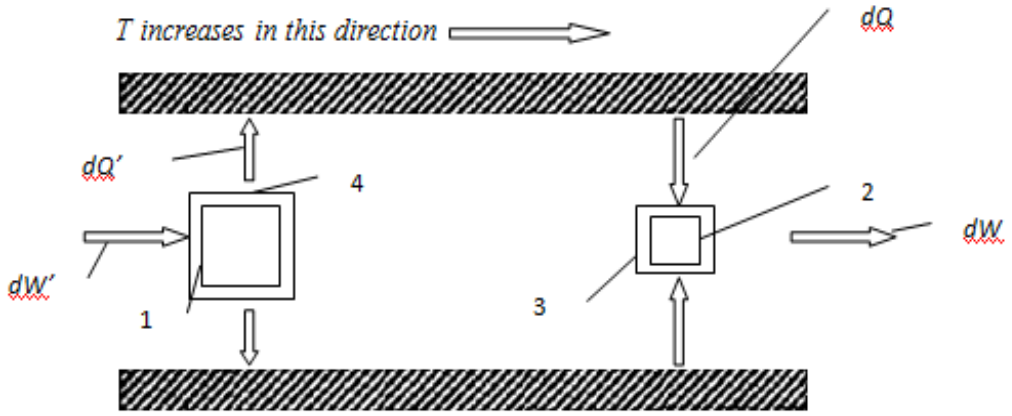

Figure 1.3: Prime mover, Lagrangian view point

This change is due to two factors: adiabatic expansion and compression of the fluid in a sound wave, and the temperature of the plate. The heat flow between the fluid and the plates does not create instantaneous change in the temperature of the fluid due to poor thermal contact. Instead, the heat flow between the fluid and the solid plates creates a time delay, or time phasing between the temperature, pressure, and motion, which is needed to drive the fluid through a thermodynamic cycle. Thus, simple irreversible heat transfer between the fluid and the plate operates a Thermoacoustic Prime Mover. In other words, poor thermal contact achieves the proper phasing of the temperature oscillations of the fluid. In the case of a realistic sinusoidal sound wave, the above argument applies to the parcels about thermal penetration depth δ_k from the plate. Thermal penetration depth is the distance through which heat can diffuse through the fluid during the time $1/\omega$, where ω is the angular frequency of the sound wave. Parcels of air within thermal penetration depth from the plate are in good enough thermal contact with the plate to

exchange heat with it. At the same time, they are in poor enough thermal contact with the plate to create a time delay between motion and heat transfer.

1.4 Heat and Work Interactions in Thermoacoustic Prime Movers

Figure 1.3 explains Thermoacoustic phenomenon from a Lagrangian viewpoint. During the compression phase 1-2 in an acoustic standing wave, the parcel of air is heated and is displaced along the plate. At the end of the compression phase, the temperature of the air parcel is still less than that of the plate. Heat dQ will flow into the air parcel from the plate and the parcel experiences thermal expansion 2-3 at high pressure and does work dW. During the expansion phase 3-4, the parcel of air is cooled down and is displaced along the plate. At the end of the expansion phase, the temperature of the air is still more than that of the plate and heat dQ' will flow from the parcel to the plate. The parcel experiences thermal contraction 4-1 at low pressure and work dW' is done on the parcel. In one complete cycle, the parcel does a net work $dW - dW'$. One fluid parcel displaces over a very small distance compared to the length of the plate. There are numerous such parcels along the length of the plate, each undergoing the same cycle and acquiring the same extreme position as its adjacent parcel acquired half a cycle earlier. If we follow this train of gas parcels within the thermal penetration depth from the plate, we observe that the heat is merely passed along the plate from one parcel to other while the plate serves as temporary storage medium. If we examine the same train of parcels for the work flow, we observe that each parcel has a net work output and the total work done by the gas is proportional to the length of the plate.

Introduction of a plate in a standing wave modifies the standing wave, resulting in a time-averaged heat flux near the surface of the plate, along the direction of vibration

and generation or absorption of acoustic power near the surface of the plate. Swift (1988) made simplified assumptions to derive the above-mentioned effects. These include:

1. The plate is short enough and far enough from both velocity and pressure nodes that pressure and velocity can be considered uniform over the entire plate
2. The fluid has zero viscosity
3. The plate has a large enough heat capacity per unit area that temperature does not change appreciably at the acoustic frequency
4. Temperature dependence of the thermophysical properties of the fluid and plate is neglected
5. Thermal conductivity of the plate and the fluid in x direction is neglected

There is a critical mean temperature gradient across the plate in the direction of vibration for which the fluid properties and standing wave geometry are such that temperature oscillations due to pressure oscillations are cancelled out by temperature oscillations which are due to displacement oscillations. This temperature gradient (Swift, 1988) is the boundary between the heat pump and prime mover functions of Thermoacoustic devices and it is given by:

$$\nabla T_{crit} = T_m \beta \omega p_1^s /\ _{\mathrm{m}} c_p u_1^s \qquad (1.3)$$

where T_m is the mean fluid temperature, β is the ordinary thermal expansion coefficient , c_p is the constant pressure heat capacity, ω is the angular frequency of the wave, p_1^s is the oscillating pressure of the standing wave, $\rho_m$is the density of the fluid, and u_1^s is the oscillating velocity of the standing wave.

The total heat flux Q_{dot} (Swift, 1988) along the plate in the x-direction is given by:

$$Q_{dot} \quad -\frac{1}{4} \quad \delta \; T_m \; p_1^s u_1^s \quad -1) \qquad (1.4)$$

where /2 is the width of the plate, δ_k is the thermal penetration depth, and = $\nabla T_m / \nabla T_{crit}$ is the ratio of actual temperature gradient to critical temperature gradient. Heat flux is proportional to the area δ and T_m (= 1 for ideal gases). It is also proportional to the product of oscillating pressure and oscillating velocity, $p_1^s u_1^s$, which implies that heat flux is zero when the plate is either at a pressure node or velocity node.

Total acoustic power W_{dot} (Swift, 1988) is given by:

$$W_{dot} \quad \frac{1}{4} \quad \delta \; \Delta x \frac{T_m \; ^2 \omega}{\rho_m c_p} (p_1^s)^2 \quad 1) \qquad (1.5)$$

W_{dot} is proportional to the volume δ Δx of the fluid within the thermal penetration depth from the plate. W_{dot} is quadratic in the acoustic amplitude and becomes zero at a pressure node. It is evident from the equation that for $\nabla T_m = \nabla T_{crit}$, there is no acoustic power, and for $\nabla T_m > \nabla T_{crit}$, acoustic power is produced and hence, the device works as a prime mover. Conversely, when $\nabla T_m < \nabla T_{crit}$, acoustic power is absorbed and the device works as a heat pump.

1.5 Structure of a Thermoacoustic Prime Mover/Laser

The prime mover studied here is a Sondhauss tube. It is a quarter wavelength prime mover. Although three different lengths of the resonators were used, the structure of all the prime movers remains the same. The length of the resonator determines the fundamental frequency of the prime mover. The structure of a quarter wavelength prime mover is as shown in Figure 1.2. It consists of a resonator, a hot heat exchanger, a cold

heat exchanger, and a stack. The prime mover used in this study does not have a cold heat exchanger and the cold part of the stack is exposed to the open end.

A resonator is a test tube with one end closed. The heat exchangers and the stack are the most important parts of Thermoacoustic devices. They drive the sound and amplify it with the help of a temperature gradient generated along the stack. Heat exchangers should be of good thermal conductance in order to efficiently transfer heat. A stack has to sustain a temperature gradient and should be made of a good heat insulating material. Optimum spacing between individual plates of a stack depends on thermal penetration, which in turn depends on the frequency of the resonator. Thermal penetration depth (Swift, 1988) is the distance in which heat can diffuse through the fluid during the time $1/\omega$ and it is given as:

$$\delta = \sqrt{\frac{2K}{\sigma c_p \omega}} \qquad (1.6)$$

where K is the thermal conductivity of the fluid, σ is the mass density of the fluid, c_p is the specific heat per unit mass of the fluid, and ω is the acoustic angular frequency.

Since no shaft work has been produced from the Thermoacoustic devices studied under this research, the Thermoacoustic Prime Movers will be referred to as Thermoacoustic lasers.

CHAPTER 2

LITERATURE REVIEW AND MOTIVATION

Thermoacoustic phenomena were first observed by European glassblowers over 200 years ago. Glassblowers heard sound when a cold glass tube was placed next to a hot glass stem. Glass tubes exhibiting such phenomenon with one end closed were named Sondhauss tubes after the scientist Sondhauss who studied these effects for the first time. Lord Rayleigh (1878) qualitatively analyzed the Thermoacoustic effect in his book, The Theory of Sound. About 150 years later, Rott and his coworkers (1980) did an accurate quantitative discussion on the Thermoacoustic effect. Feldman (1968) commented that the most important milestone in experimental thermoacoustics came in 1962 when Carter and his coworkers realized that the efficiency of Sondhauss tubes can be improved by introducing a solid structure, a stac , inside the resonator. Feldman's Ph.D thesis research (1966) was based on this and he successfully produced 27 W of acoustic power from 600 W of heat.

Lord Rayleigh (1878) gave a qualitative explanation for the acoustic power production with unsteady heat transfer to the compressible fluid in terms of the relative phase of the pressure wave and the heat transferred to the fluid.

> In almost all cases where heat is communicated to a body, expansion ensues, and this expansion may be made to do mechanical work. If the phase of the forces thus operative be favorable, a vibration may be maintained…. For the sake of simplicity, a tube, hot at the closed end and getting gradually cooler towards the phase of greatest condensation… the air is moving inwards, i.e., towards the

> closed end, and therefore is passing from colder to hotter parts of the tube; … But in fact the adjustment of temperature takes time, and thus the temperature of the air deviates from that of the neighboring parts of the tube, inclining towards the temperature of that part of the tube from which the air has just come. From this it follows that at the phase of greatest condensation heat is received by the air, and at the phase of greatest rarefaction heat is given up from it, and thus there is tendency to maintain the vibrations.

In quantitative terms, it means that a wave is promoted if the absolute value of this relative phase is less than $\pi/2$. Guadalupe Huelsz and Eduardo Ramos (1999) experimentally verified Rayleigh's interpretation of acoustic power production.

Guadalupe Huelsz and Eduardo Ramos (1996) analyzed Rayleigh's qualitative interpretation of Thermoacoustic effects based on the linear theory developed by Rott (1980) and Swift (1988). They calculated the phase difference between the pressure and the heat supplied to the fluid. They also derived the expression for time-average power produced ($W>0$) or absorbed ($W<0$). The results shown by Guadalupe Huelsz and Eduardo Ramos (1996) prove that acoustic power is generated when pressure perturbations and heat perturbations are in phase, and the acoustic power is absorbed when pressure perturbations are out of phase with the heat perturbations. This verifies Rayleigh's theory (1878) quantitatively. The authors showed that the time-average power produced, which is an integral quantity, is proportional to the time-average product of the pressure perturbations and heat perturbations, which are both local quantities. This showed that the Thermoacoustic phenomenon is controlled by the conditions at the fluid-solid boundary.

G. W. Swift (1988) discussed fundamentals of Thermoacoustic engines in detail by analysis and by discussing examples of Thermoacoustic convertors. Swift illustrated the basic principles of Thermoacoustic engines by considering an example of a single

small solid plate aligned parallel to the direction of vibration of an acoustic plane standing wave. The author pointed out that with the introduction of a solid plate in a standing wave, the standing wave was modified, resulting in two very important effects: " 1) A time averaged heat flux near the surface of the plate, along the direction of acoustic vibration, and (2) the generation or absorption of real acoustic power (work) near the surface of the plate." The author made many simplifying assumptions to derive these two basic effects for the simple example of a single plate introduced in a standing wave. Later in the paper, derivations were made for more complicated real-life situations. Expressions for the critical temperature gradient, total heat flux along the stack, and total acoustic power produced derived by the author prove that the introduction of a solid stationary body in a standing wave stimulates the heat flux along the stack. The heat flux is about a thermal penetration depth from the solid boundary and the production or absorption of acoustic power by the fluid near the solid boundary.

A recent work on the linear theory on Thermoacoustic by Roger Waxler (2001) assesses second-order time-averaged acoustics of a viscous, thermally conducting gas between closely spaced parallel plates. The author focused on the relation between the time-averaged mass flux and pressure gradient and obtained an explicit expression between time-averaged pressure drop across a Thermoacoustic stack and time-averaged mass flux through the stack.

The stack is one of the most important components of Thermoacoustic devices. One of the problems faced by researchers in the past was the inability to explore the effects of various geometric factors of the stack, including length, spacing, and general geometry. This was due to the difficulty of making stacks by hand. In a recent study,

Ryan Lampe (2008) used Selective Laser Sintering to produce several different stack arrays such as square tubes, parallel plates, and a pin array. These fabricated stacks were then tested and their performances were compared using a compressor-driven closed-tube heat pump. It was observed that the drop of 4.3 C can be obtained across a parallel plate stack using a 12-W amplifier, with 130mV peak-to-peak of the sine wave audio signal. Using the fabrication techniques discussed in this paper, stack designs with 0.5 mm spacing could be manufactured. This work opened gates for better understanding of stack design on efficiency of Thermoacoustic devices.

Yong Tae Kim and Min Gon Kim (2000) studied stack position dependency of the temperature dependency across the stack. The authors measured acoustically produced temperature difference across the stack as the function of stack position and sound frequency. The measured positional variation of ΔT across the stac matched empirical relations derived by Wheatley and coworkers (1983) when the stac length Δx was replaced by a fractional quantity $\alpha\Delta x$. This is because the actual temperature distribution across the stack is skew S-shaped with constant temperature plateaus at both ends.

Placement of the stack within the resonator is also important in terms of efficiency. The rate of heat transfer is directly proportional to acoustical velocity. Applying the principle of superposition, Fahey (1992) suggested placing the maximum heat gradient at the point of maximum gas molecule velocity. In Thermoacoustic devices, the maximum gas molecule velocity appears at approximately one third of the tube length from the closed end.

The stack forms the heart of a Thermoacoustic heat pump and recent researchers have focused more on stack geometry to improve the performance of theroacoustic devices. Tijani, Zeegers, and Waele (2002) reported quantitative experimental investigation of the effect of pore dimensions on the performance of Thermoacoustic devices. They manufactured parallel plate stacks with stack spacing varying from 0.15 mm to 0.7 mm and measured the performance of Thermoacoustic refrigerators with these stac s. It was reported that the sheet spacing of $2.5\delta_k$ in a stack should be optimum for cooling power. The results were also confirmed by DALTAE (Ward & Swift, 2001) calculations. DALTAE is a computer program which resolves theroacoustic linear equations for a specified geometry.

G. Bisio and G. Rubatto (1999), after reviewing the literature on thermoacoutics, described actual and possible applications of the Sondhauss oscillations in 1998. One of the possible applications is generation of electric power. A Thermoacoustic converter can generate alternating current electricity by steady heat input into a conducting gas oscillating in a magnetic field. Feldman's (1966) experimental studies obtained high sound pressure levels from 100 to 145 dB, with heat inputs from 200W to 600W. G. Bisio and G. Rubatto (1999) predicted possible applications of these oscillators for generation of high-intensity acoustic fields for environmental tests or acoustic beacons. Feldman (1966) also proposed the use of Sondhauss oscillators as a driver for an alternating current MHD generator. Thermoacoustic phenomena could be the reason for intense acoustic vibration experienced in heat exchanger and steam generator tube banks. Bisio and Rubatto (1999) point out that the study of fluid-Thermoacoustic vibrations in

vertical gas turbine recuperators might be used for selecting vibration-resistant configuration.

Symko and his coworkers (2004; 2010) suggested the use of Thermoacoustic Prime Movers for thermal management and electrical energy generation in the systems which are sources of heat. The quarter wavelength Thermoacoustic Prime Movers developed by Symko generated sound waves of frequency up to 24kHz. The sound generated by these prime movers was then converted to electricity using a 3 cm diameter piezoelectric material, PZT, in the unimorph configuration, thus providing thermal management and electrical energy generation.

Because of the mechanical simplicity of Thermoacoustic devices, Garrett and Backhaus (2000) predicted that Thermoacoustic devices could be used for generating electricity at individual homes, for producing domestic hot water, and for producing space heating and cooling. Thermoacoustic refrigerators have already been operated on the space shuttle and aboard a Navy warship.

Continued research in the 1980s and 1990s (Swift 2004) to understand the phenomenon of thermoacoustics led to improvement in Thermoacoustic efficiency with the introduction of regenerators, couples, and modified tube structures. The invention of the free-piston in 1970 began an important phase in the development of Stirling engines and refrigerators. This eliminated dependence on crankshafts and connecting rods for piston motion, which could be determined by piston dynamics and gas dynamics. Ceperley (1979) realized that the time phasing between pressure and motion oscillations in the heart of regenerators of Stirling engines and refrigerators is that of a travelling acoustic wave. This paved the way for the development of thermoacoustic-Sterling

engines, which find application in spacecraft power and combined-heat-and-power systems on earth. One more important application of the Thermoacoustic phenomenon is gas mixture separation. Radial oscillating thermal diffusion and axial oscillation's viscous motion in a gas mixture create a time-averaged separation of the components of gas mixture along the length of the tube.

Acoustic energy generated by Thermoacoustic Prime Movers could be used for a variety of other applications. Ultrasounds are used in medical fields to break kidney stones or for treating tumors. Acoustic energy is also used for sanitizing liquids and for cleaning and sterilizing surfaces and medical instruments. Recent developments in thermoacoustics and the possibility of utilizing waste heat or solar energy for running Thermoacoustic devices make it technically promising and economically sound to generate large quantities of acoustic energy.

The growing popularity of thermoacoustics and the associated recent developments were the chief motivating factors behind our investigation of Thermoacoustic Prime Movers. Despite the aforementioned work, studies that have attempted to understand the effects of geometric parameters of Thermoacoustic Prime Movers on acoustic output are scant. Accordingly, the primary aim of this research was to generate large quantities of high amplitude sound waves by varying different geometric parameters, including the stack length, the stack position, and the length of the resonator.

CHAPTER 3

EXPERIMENTAL SETUP AND PROCEDURES

3.1 Construction of a Thermoacoustic Laser

The goal of this thesis was to identify the optimum operating conditions of a Thermoacoustic laser for maximum acoustic power. Geometric variables, including the stack position, the stack length, and the resonator length, were varied and the acoustic output was measured. The dependence of acoustic output on electric input was also observed. The Acoustic Laser kit (2000) provided by the Penn State Graduate Program in Acoustics was used for all experimental purposes. The kit consists of a Pyrex test tube as a resonator, a Celcor ceramic catalytic converter as a stack material, and 26 gauge Nichrome (NiCr) resistance heater wire. A 24 gauge copper magnet wire with enamel insulation was used for making necessary electrical connections. The stack was heated with the help of a Nichrome (NiCr) wire wound on one side of the stack and the other part was cooled by radiation and natural convection to the atmospheric air.

The stack was made from a rectangular Celcor ceramic catalytic converter. Ideally, the cross-section of the stack should be circular, but an approximate octagonal shape with smoothened edges was carved out of the original converter. A hacksaw and sandpaper were used to reshape the ceramic converter. The stack was made so that it nearly filled the tube and was able to easily slide in and out of the tube. The original ceramic catalytic converter and the stack made from it are shown in Figure 3.1.

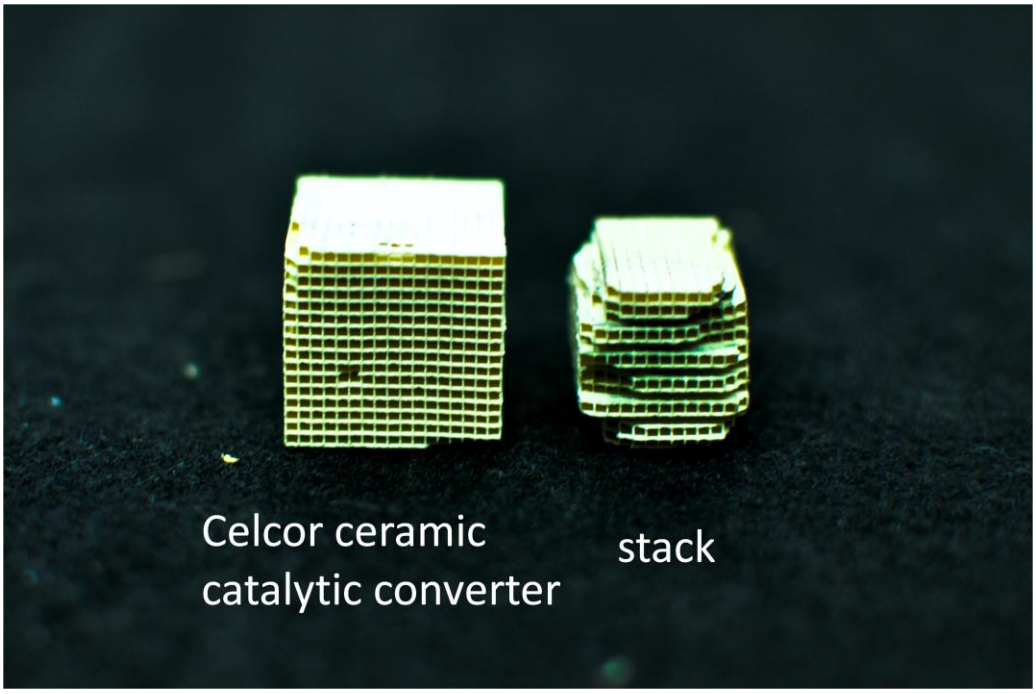

Figure 3.1: Original Celcor ceramic catalytic converter and the stack

The next step was to make grooves on the ceramic stack for placing heater wires. Six grooves about 3 mm deep were made on the top surface of the stack with the help of a hacksaw and sandpaper. These grooves contained the serpentine Nichrome (NiCr) heater wire. Two copper wires of length 60 cm were stripped by burning the enamel coating and were inserted through one of the channels of the ceramic stack. The exposed part of the copper wire was then twisted with the Nichrome (NiCr) wire to make a good electrical contact. In order to ensure a good mechanical and electrical contact, cylindrical crimp connectors were slipped through the twisted Nichrome and copper wires and were crushed tightly around them. This whole assembly was then inserted into the glass tube. The copper wires were fixed on the outer surface of the tube with the help of tape to prevent the stack from moving within the tube in the axial direction. The stack with the heater wire wound on its side is shown in Figure 3.2:

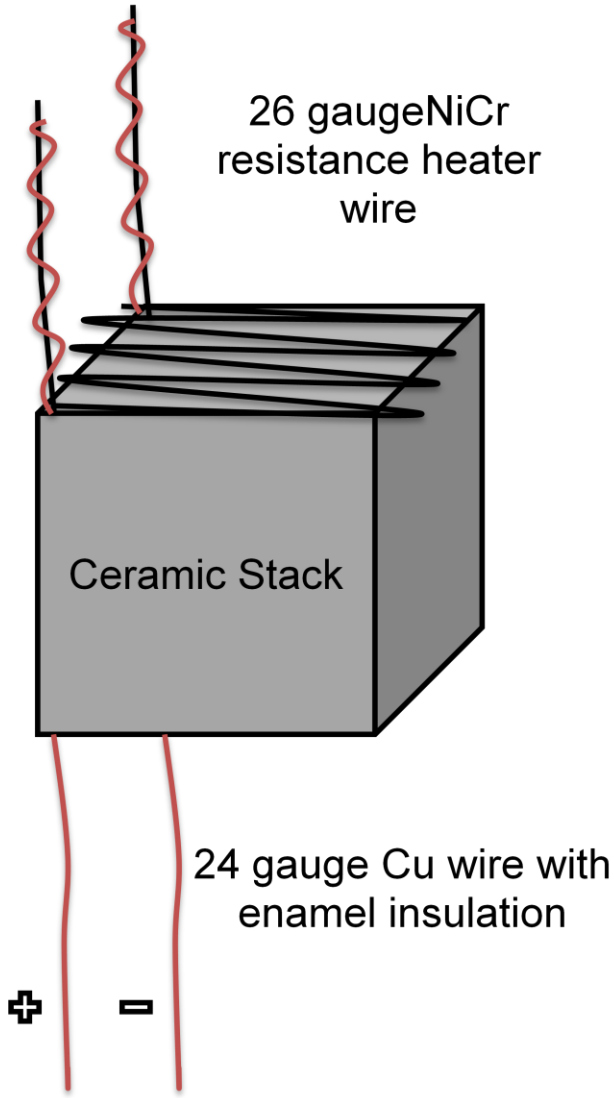

Figure 3.2: Stack and the heater wire assembly

3.2 Experimental Setup and Electrical Connections

Thermoacoustic lasers were made following the procedures mentioned in Section 3.1. Three different lengths of resonators were tested, including 10 cm, 15 cm, and 20 cm. These resonators were also tested for different lengths of stack materials within the resonator. Stack positions were also varied within the resonator to observe optimum position for producing maximum acoustic power output. Different experimental conditions considered to find the optimum operating conditions of a Thermoacoustic laser are listed in Table 3.1, where d is the distance of the stack measured from the open end of the tube, l is the length of the stack material, and L is the length of the resonator.

Electrical connections for a Thermoacoustic laser for all these setups were the same, as shown in Figure 3.3. Input voltage was varied by changing the resistance value of a variable resistance. A CEN-TECH 98025 multimeter was used to measure the voltage across the Nichrome (NiCr) wire and connecting copper wires. Specifications for the multimeter are mentioned in the Appendix.

Voltage across the Nichrome wire was then calculated by applying Kirchhoff's Law and by measuring the resistances of connecting copper wires and a Nichrome (NiCr)

Table 3.1: Different conditions for conducting the experiments

	d (cm)	l (cm)	L (cm)	Input Voltage (V)	Length of heater wire used (cm)
Case I	2, 4, 6, 8..	1.25, 2.5	15, 20	5.5 V, 6 V	13.5
Case II	L/4	1.25, 2.5, 5	15, 20	5.5 V, 6 V	15.5
Case III	L/4	2.5	15, 20	5.5 V, 6 V	15.5
Case IV	L/2	1, 1.25	2.5, 5, 7.5, 10, 20	6 V, 6.5 V	15.5

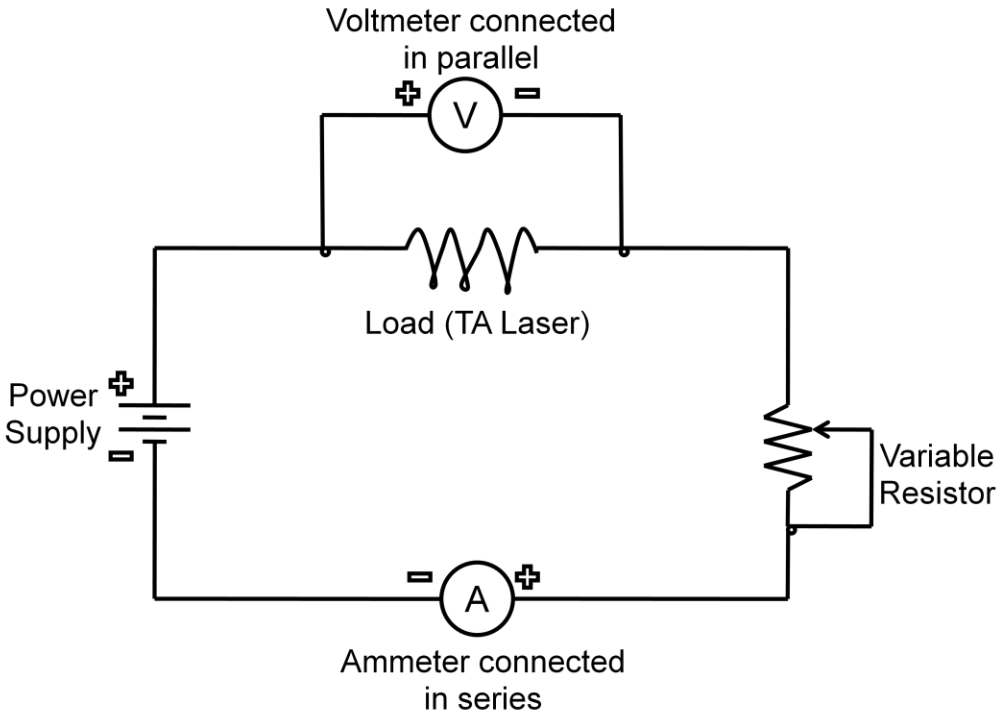

Figure 3.3: Electrical connections for a Thermoacoustic laser

wire. Voltage across the Nichrome wire thus calculated and the measured resistance of the Nichrome wire were used to calculate power consumption of the Thermoacoustic converter.

$$P = \frac{V^2}{R} \tag{3.1}$$

The voltage across the Nichrome wires increased slightly when the Thermoacoustic converter was heated up, indicating the Nichrome wire resistance changed with temperature. For this reason, the voltage values within the circuit were monitored every 30 seconds to observe any change in the power consumption.

3.3 Sound Pressure Level (SPL) Measurements

A Tenma 72-942 sound level meter was used to measure the sound pressure levels of the Thermoacoustic laser. This unit conforms to the IEC651 type 2, ANSI S1.4 type 2 for sound level meters. Specifications of the same are given in the Appendix.

Measurements were taken 10 cm away from the tube opening and along the axis of the glass tube to avoid any disturbance due to sound level meter blocking and by aligning the microphone with the axis of the resonator tube. Frequency weighting C was used to make all the measurements. For measuring the average sound pressure levels, the time weighting was kept in SLOW mode. Maximum sound pressure levels were measured by keeping the time weighting in FAST mode and by turning on the maximum hold option of the sound level meter. Experimental setup for measuring the sound pressure level is shown in Figure 3.4.

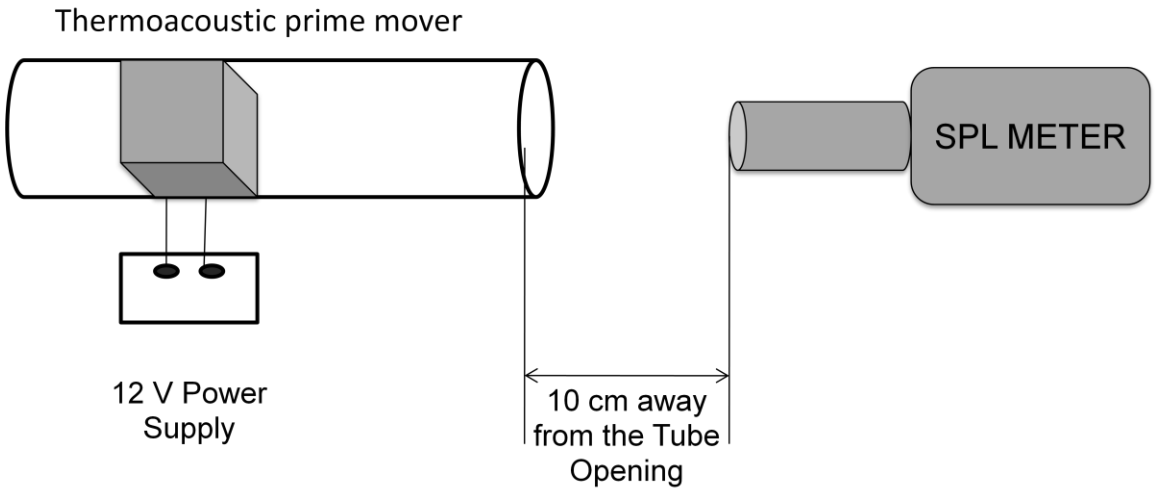

Figure 3.4: Experimental setup for measuring sound pressure level

3.4 Working with LabVIEW SignalExpress

Three different lengths of test tubes were tested to observe the effects of the length of the resonator on the output frequency of a Thermoacoustic laser. A National Instruments data acquisition (DAQ) device, NI USB 6009, was used to acquire the signal. Specifications of NI USB 6009 are given in the Appendix. The NI USB 6009 provides connection to eight analog input (AI) channels, two analog output (AO) channels, 12 digital input/output (DIO) channels, and a 32-bit counter with a Full-Speed USB interface. Analog terminal assignments for NI USB 6009 are shown in the Appendix. The positive lead of the electrical signal generated with the unidirectional microphone was connected to AI 0+ terminal and the negative lead was connected to AI 0- terminal. To read the frequency of a themoacoustic laser, a unidirectional microphone was used. A microphone is an acoustic-to-electric transducer which converts sound into electrical signal. An omnidirectional microphone picks up sound from all directions and responds evenly to it. This quality is not desired for reading sound from a subject at a distance while conducting scientific experiments. A unidirectional microphone is sensitive to sound only from one direction, thus eliminating ambient noise from the side and rear. The experimental setup for acquiring the signal using NI USB 6009 is shown in Figure 3.5.

LabVIEW SignalExpress was used for analyzing the data acquired using the DAQ device. SignalExpress can acquire, generate, analyze, compare, import, and log signals. LabVIEW SignalExpress can be used to define measurement procedures by adding and configuring steps in an interactive measurement environment. A step is a configurable function that acquires, generates, analyzes, loads, or stores signals. Three steps were used for the analysis. The DAQmx Acquire step was used for acquiring the signal, Distortion

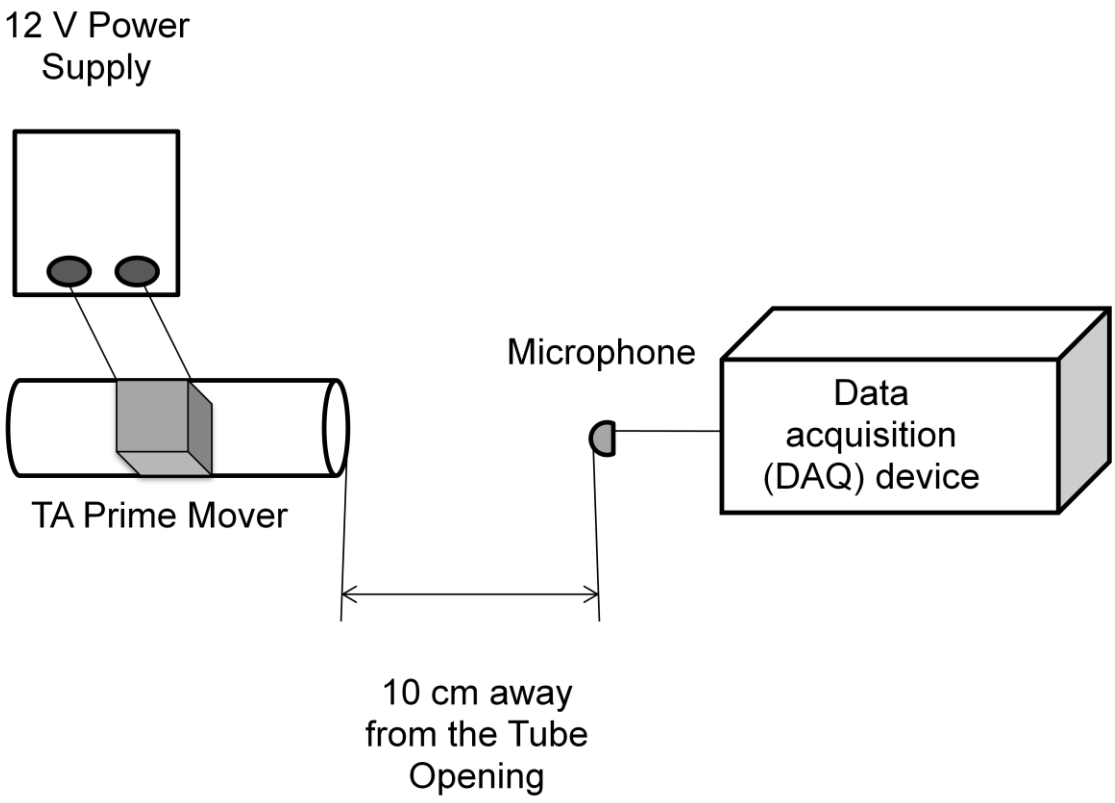

Figure 3.5: Experimental setup for acquiring and analyzing the acoustic signal

step for observing the frequency of the oscillations, and Amplitude and Level step for measuring rms value of the voltage generated by the microphone. Sampling frequency of 20 kHz was used to ensure that enough data points were available to define one complete cycle of the wave for high-frequency prime movers.

3.5 Details of Experiments

As mentioned before, multiple sets of experiments were conducted to check acoustic output of a Thermoacoustic laser by varying stack position, stack length, input power, and length of a resonator. All electrical connections were made as mentioned in Section 3.2. For all sets of experiments to identify optimum operating conditions for a

Thermoacoustic laser, the flowchart shown in Figure 3.6 was followed. Readings were taken when the output of the Thermoacoustic laser was stabilized. Maximum and average values were recorded separately. The Thermoacoustic laser was allowed to cool down between two consecutive readings by turning off the system for a minimum of 2 minutes. This was necessary to avoid the possibility of burns while changing the variables like stack position and stack length. Three different stack lengths (12.5 mm, 25 mm, and 50 mm) were examined to check the effects of stack length on the performance of a Thermoacoustic laser. The 12.5 mm stack was made by cutting the 25 mm stack with the help of a hacksaw. The 50 mm stack was made by placing two stacks of 25 mm length close to each other such that the pores of both the stack materials are aligned properly. More observations were made by changing the input voltage values for the Thermoacoustic laser. Sometimes, the wires shorted out or broke at the junction of the copper wire and NiCr wire due to contact resistance. The wires were replaced with the exact lengths of the same materials whenever it was necessary to maintain consistency in the results.

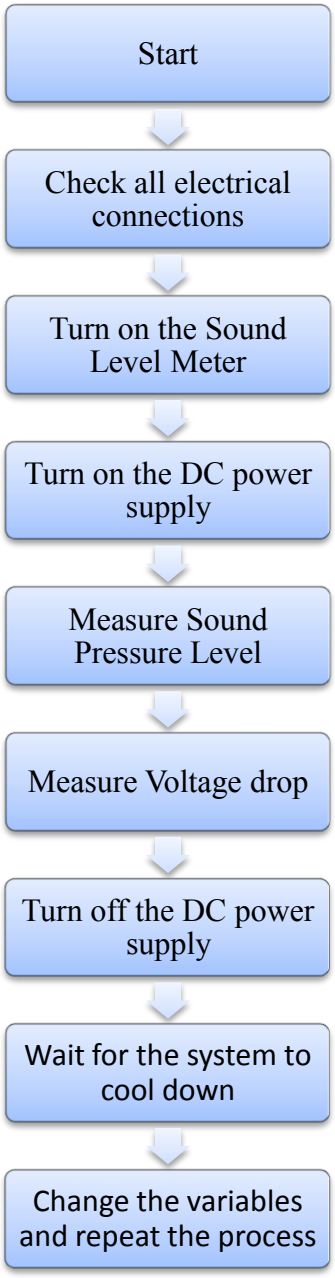

Figure 3.6: Flowchart for conducting experiments

CHAPTER 4

RESULTS AND DISCUSSIONS

4.1 SPL vs Distance from the Tube Opening

Sound pressure level measurements were taken by arranging the SPL meter in three different orientations (0^o, 45^o, and 90^o), as shown in Figure 4.1. SPL measurements were also taken by varying the distance of the SPL sensor from the tube opening in these directions. Data were recorded for two different input voltage values and the results, as discussed below, were consistent in both cases.

Sound pressure levels decreased rapidly with distance after exiting the tube opening and remained almost the same at a great distance from the tube opening. SPL readings in different directions differed only slightly. The assumption of a spherically spreading wave is thus valid. A slight increase in sound pressure level was observed at a distance of about 1/2 wavelength from the tube opening. Theoretically, the air displacement amplitude is highest at this position in a plane standing wave. The SPL meter recorded the highest sound pressure levels at the tube opening, which is a pressure node. In a standing wave, pressure (static) oscillations are zero at the tube opening and flow velocity oscillations are the highest. Oscillations in dynamic pressure are due to the deceleration of air flow when the flow impacts the SPL meter surface.

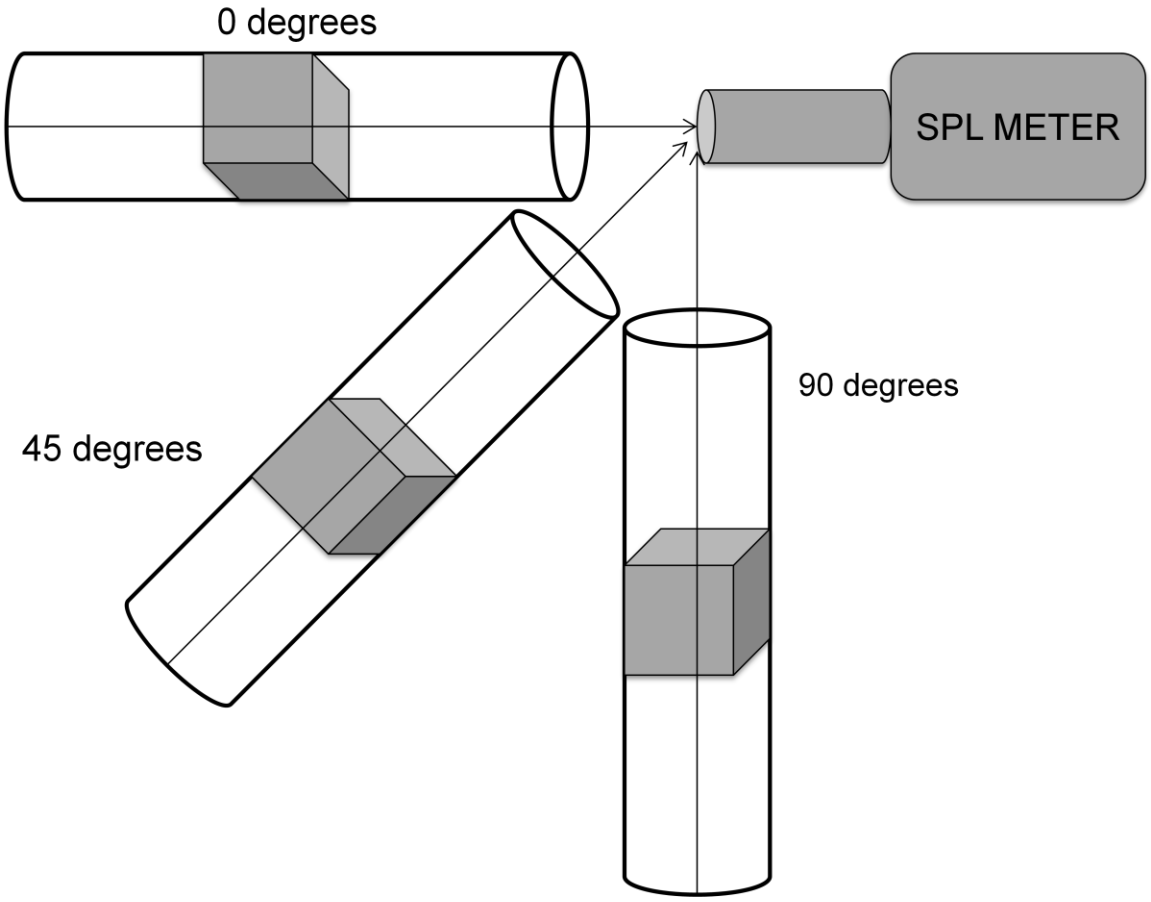

Figure 4.1: Experimental setup for measuring SPL readings in three different orientations.

The SPL meter measured the intensity of the total (static plus dynamic) pressure fluctuations. As the distance from the tube opening increased, the SPL readings decreased and at a distance of ½ wavelengths from the tube opening, the SPL reading slightly increased. This point is a pressure node point for a plane standing wave, as shown in Figure 4.2. This indicates that the dynamic pressure oscillations contributed more to the SPL readings than the static pressure oscillations. Figure 4.3 shows these experimental results. Case 1 shows results for input voltage V = 5.66 V and Case 2 for input voltage V = 5.15 V.

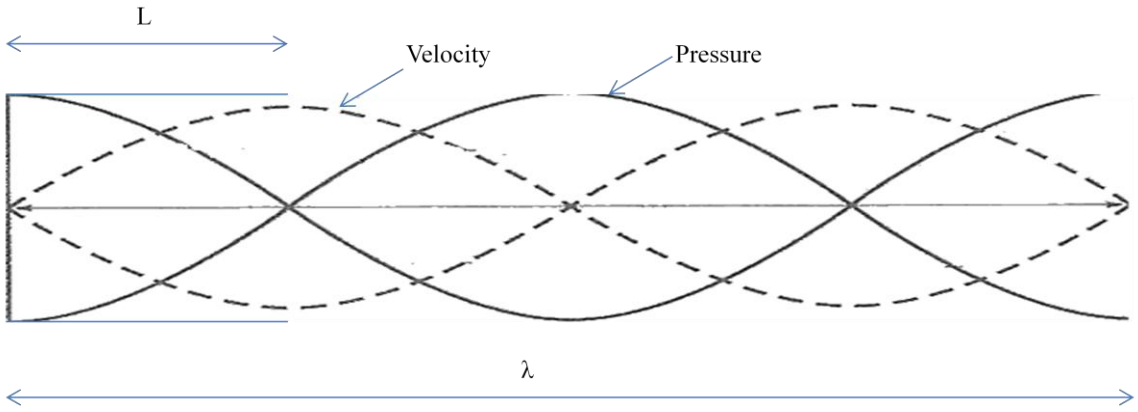

Figure 4.2: Quarter wavelength prime mover with one end closed. The solid line corresponds to the pressure of the standing wave and the dotted line corresponds to the velocity of the air particles in the standing wave.

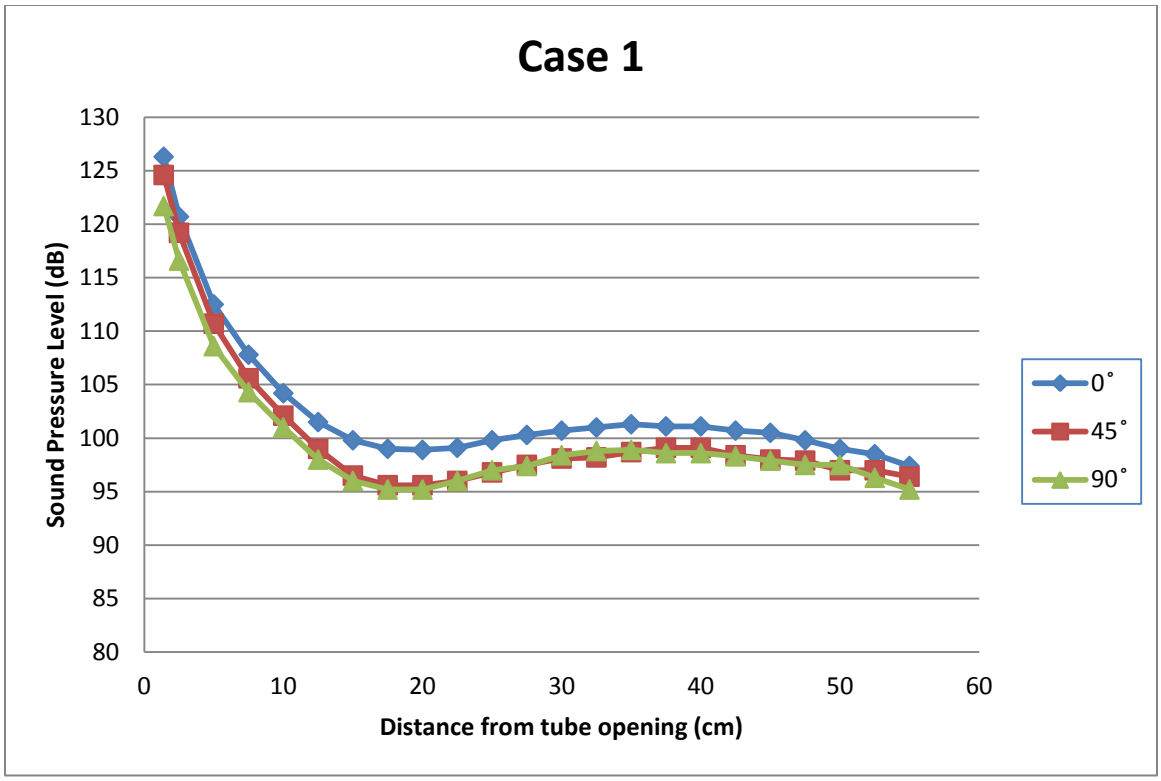

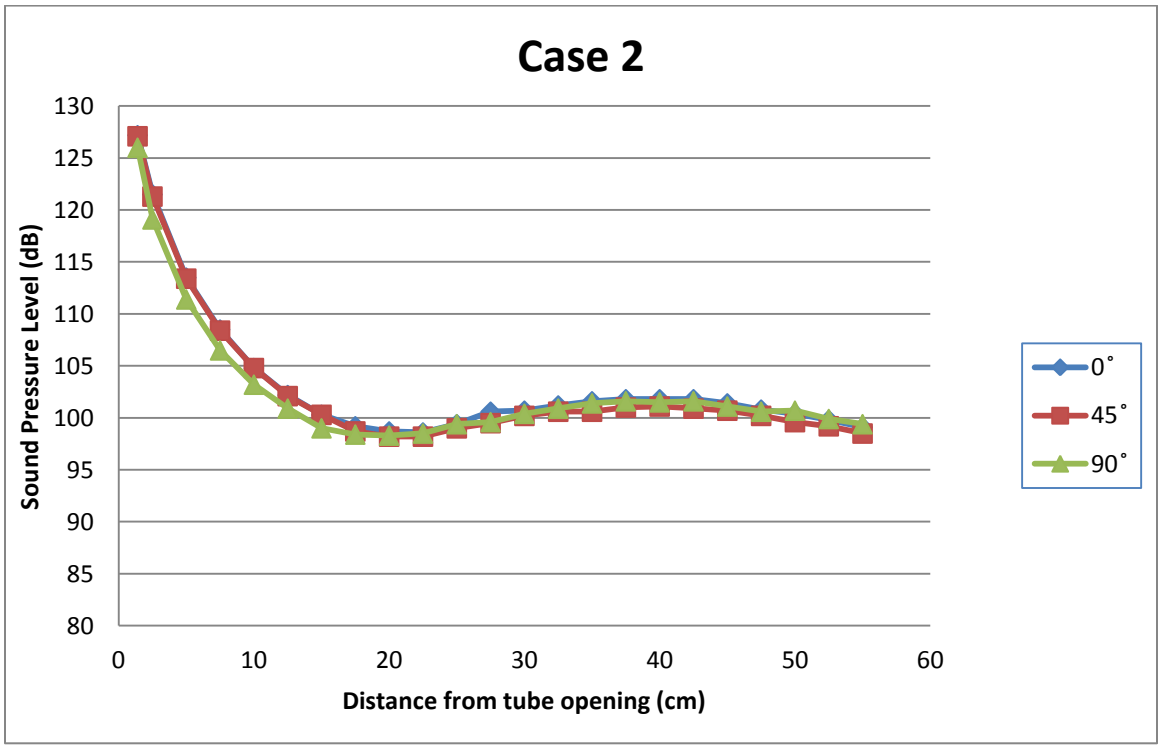

Figure 4.3: SPL measurements vs distance from the open end of the prime mover.

4.2 SPL vs Stack Position

Geometrically, the Thermoacoustic lasers studied in this work are quarter wavelength prime movers. These are simple in construction and are cylindrical in shape with one end closed. The resonator was made of a cylindrical glass tube and the stack was made from a ceramic catalytic converter. These resonators are standing wave prime movers. In these resonators, the sound pressure node is at the open end and the sound pressure antinode is at the closed end of the resonator; hence, they excite odd integer resonant frequencies. The resonant frequency depends on the length of the Thermoacoustic laser. The fundamental resonant frequency is given by:

$$f_o = a/\lambda \tag{4.1}$$

where a is the speed of sound and λ is the wavelength. For a quarter wavelength prime mover of length L, λ is given by:

$$\lambda = 4L \tag{4.2}$$

A 15 cm long quarter wavelength Thermoacoustic laser and a 20 cm long quarter wavelength Thermoacoustic laser were tested to check the optimum position of the stack within the resonator. The position of the stack was measured from the closed end of the resonator, as shown in Figure 1.2, and along the axis of the glass tube. Three different stacks with thicknesses of 12.5 mm, 25 mm, and 50 mm were used in the experiments. The results are presented in Figure 4.4, Figure 4.5, and Figure 4.6. The results were consistent in all the cases with optimum stack position being approximately 1/4th of the tube length from the closed end of the resonator.

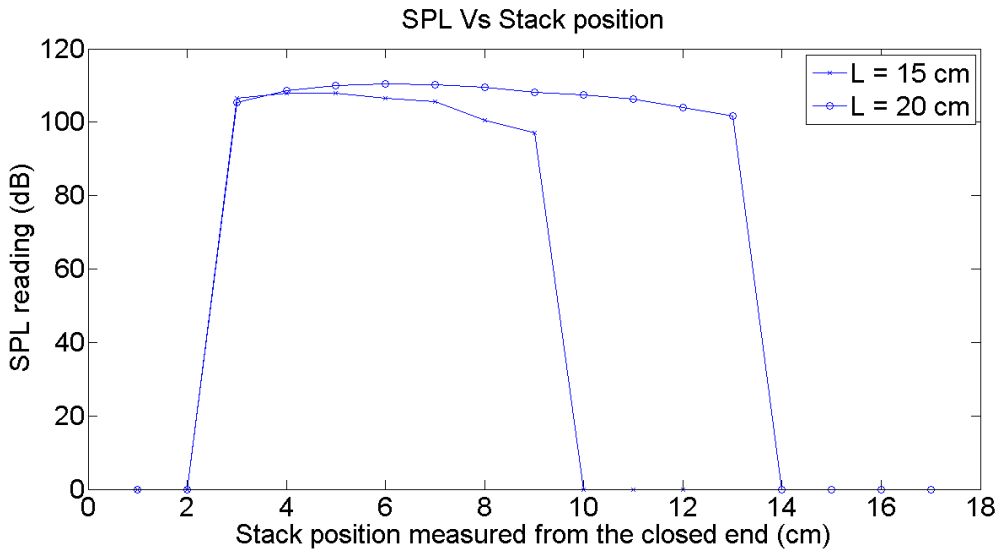

Figure 4.4: SPL vs Stack position for tube length, L = 15 cm and L = 20 cm with stack length l = 2.5 cm

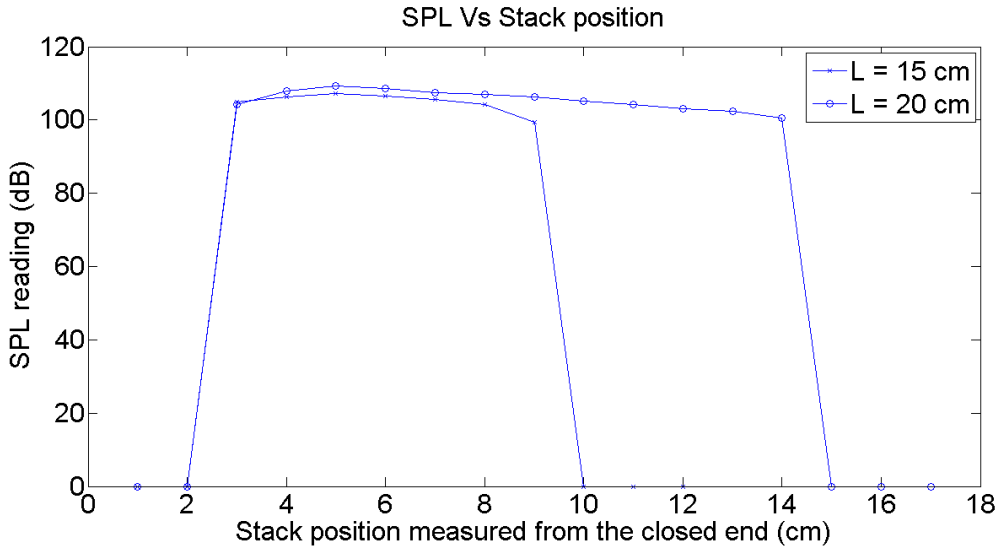

Figure 4.5: SPL vs Stack position for tube length, L = 15 cm and L = 20 cm with stack length l = 1.25 cm

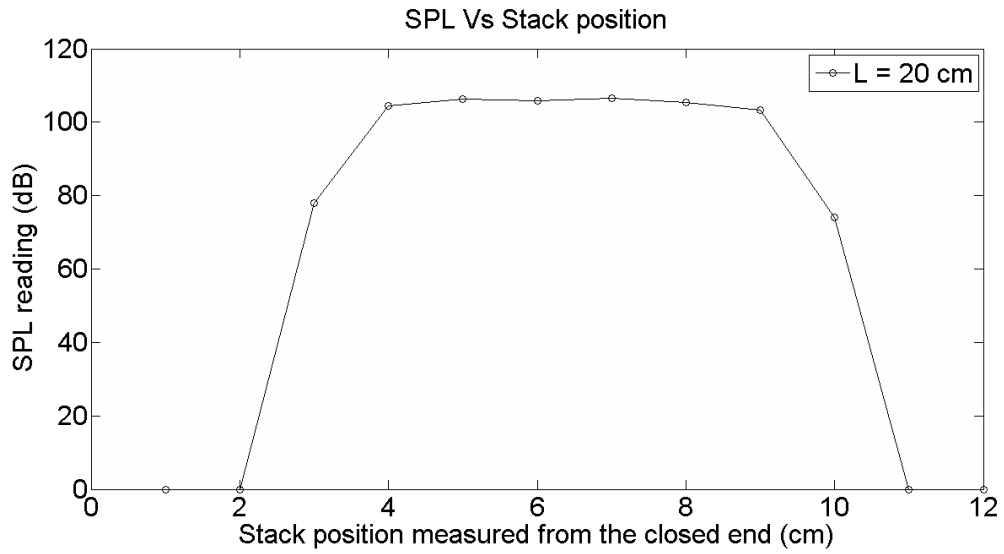

Figure 4.6: SPL vs Stack position for tube length, L = 20 cm with stack length l = 5 cm

The effects of stack position on acoustic intensity were previously studied by Young Sang Kwon (2006). According to Kwon, the theoretical optimum position of a stack is near the midpoint of a prime mover. The acoustic power output of a prime mover is given by equation 1.8. According to this equation, the power output is proportional to the product p_1u_1, which is the acoustic intensity. This product reaches maximum value at the midpoint of the prime mover. An experimental investigation by Kwon (2006) revealed that the maximum output is between a third and a half of the length of the prime mover from the closed end. The author points out that this shift in the position of maximum output towards the closed end is due to the interaction of the resonator with the outside air at the open end. Experimental data collected in this investigation suggest that, even though the maximum output is at a quarter of the length of the prime mover from the closed end, the output remains fairly constant between a quarter and a half of the length of the prime mover from the closed end.

4.3 SPL vs Stack Length

The core and the most important part of a Thermoacoustic laser is its stack. The Thermoacoustic phenomenon occurs in a small thermal boundary layer δ_k) next to the plates of the stack material. Ideally, the distance between two adjacent plates in the stack should be $2\delta_k$. Researchers were not able to explore the effects of factors like stack geometry, length, and spacing in the past. Ryan Lampe (2008) fabricated several functional Thermoacoustic stacks using rapid prototyping. These stacks could easily be fabricated and tested to compare theoretical and experimental results.

The scope of this research was to explore the effect of stack length on the acoustic output of the Thermoacoustic lasers. Spacing between the plates of the stack was not varied due to the complexity of fabrication techniques. However, a recent study by Tijani (2002) has shown that the optimum spacing between two stack plates for a parallel plate stac shoul d be $3\delta_k$.

For these experiments, the stack was positioned at L/4 distance from the closed end, which was observed to be the optimum stack position for producing maximum output in quarter wavelength prime movers. Sound pressure level was recorded at a distance of 10 cm from the tube opening and along the axis of the tube. The maximum and average values of sound pressure levels increased with the stack length. The effect of stack length on acoustic output was observed in both 15 cm long and 20 cm long Thermoacoustic lasers and the results are presented in Table 4.1. The results are presented in Figure 4.7 and Figure 4.8 and were consistent in both sets of experiments.

Table 4.1: Sound pressure level measurements for different stack lengths (L is the length of the tube, l is the length of stack, r is distance from tube opening, and V_{in} is input voltage)

Experimental Setup	SPL in dB (Max) for l = 1.25cm	SPL in dB (Average) for l = 1.25 cm	SPL in dB (Max) for l = 2.5 cm	SPL in dB (Average) for l = 2.5 cm
L = 15 cm, V_{in} = 6.28V, r = 10 cm	109.1	107.5	109.5	108.6
L = 20 cm, V_{in} = 6.35V, r = 10 cm	107.5	105.2	109.3	108.5

Total acoustic power produced in a Thermoacoustic laser is given by equation 1.8 (Swift 1988). The acoustic power is proportional to the volume $\delta\ \Delta x$. $\delta\ \Delta x$ is the volume of the fluid present within the thermal penetration depth from the plate. As the stack length Δx increases, this volume increases. The acoustic power is also proportional to $= \nabla T_m / \nabla T_{crit}$, the ratio of actual temperature gradient to critical temperature gradient. When the stack length is increased and the input power is kept the same, the temperature gradient ∇T_m decreases. Thus, increasing the stack length creates two effects: 1) the volume of the fluid within the thermal penetration depth from the plate surface increases, which increases the acoustic power output and 2) the temperature gradient across the stack length decreases, which decreases the acoustic power output. Under our experimental conditions, the net effect of increasing the stack length was an increase in the acoustic power output.

In order to understand this phenomenon from the Lagrangian point of view, consider a parcel of fluid in the thermal boundary layer of the stack. A given parcel of fluid has a very small displacement of fluid with respect to the length of the plate. Thus,

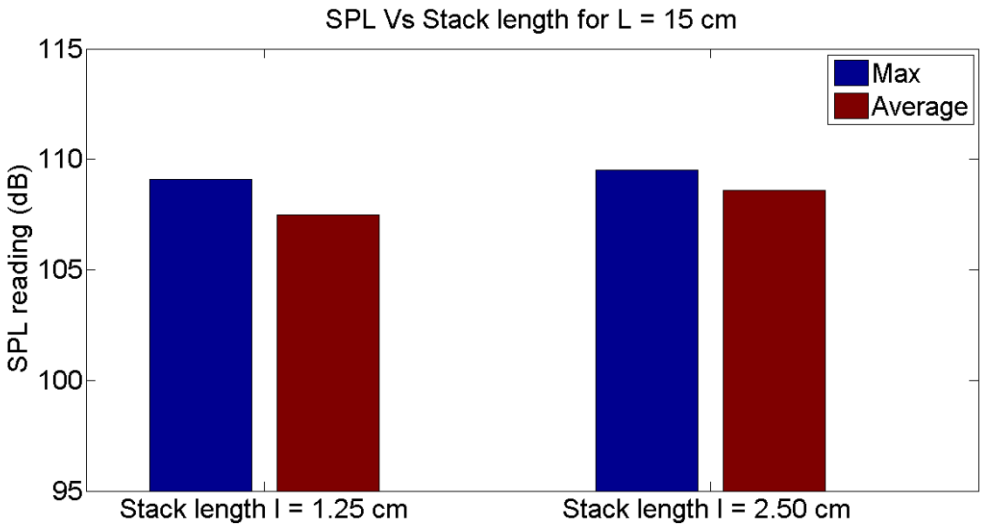

Figure 4.7: SPL (max and average) vs Stack Length for tube length L = 15 cm

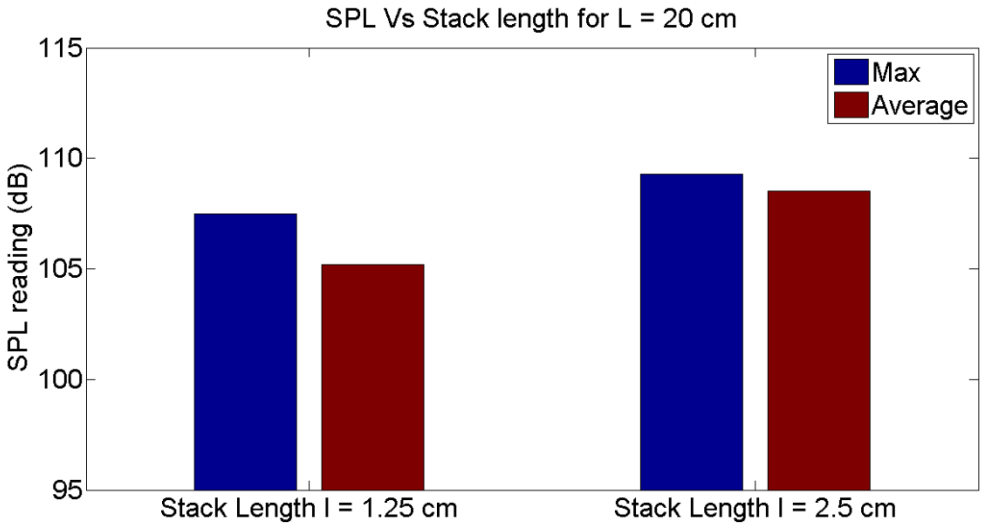

Figure 4.8: SPL(max and average) vs Stack length for tube length L = 20 cm

there is a train of adjacent fluid parcels oscillating in a short region and each has its fixed extreme positions, as occupied by its adjacent parcels half a cycle before. Each parcel of gas, near the plate in the thermal boundary level, undergoes expansion at lower pressure and contraction at higher pressure, and thus, has net work done on it. Hence, the total work done on the gas is proportional to the length of the plate.

4.4 SPL vs Tube Length

Two Thermoacoustic lasers of lengths 15 cm and 20 cm were tested by keeping the input power the same. Both the lasers used the same stack of thickness, 25 mm. The stack was positioned at the optimum position for both the converters, which was at L/4 distance from the closed end of the resonator tube. Sound pressure level readings, maximum and average, were taken at a distance 10 cm away from the open end and along the axis of the glass tube. It was observed that the longer tube recorded higher SPL readings. The results are presented in Table 4.2 and Figure 4.9.

The Thermoacoustic phenomenon is controlled by conditions at the fluid-solid boundary. This fact was ascertained by G. Huelsz and E. Ramos (1996). Time-average acoustic power production is an integral quantity proportional to the time-average product of pressure perturbations and heat flux interaction between the fluid and solid boundary. For a longer tube, even though the surface area of the stack is the same as that of the short tube, there is a greater surface area of the tube in contact with the fluid. This excess surface area also provides the stack effect, which is responsible for the higher sound pressure levels recorded from longer tubes.

Table 4.2: Sound pressure level measurements for different tube lengths (L is the length of the tube, l is the length of stack, r is distance from tube opening, d is distance of stack from closed end, and V_{in} is input voltage)

Experimenal Setup (l = 2.5 cm, V_{in} = 6.49 V)	SPL reading (dB) for L = 15 cm, d = 5 cm	SPL reading (dB) for L = 20 cm, d = 6 cm	Rise in SPL reading (dB)	Percentage rise (%)
Max Value	109.2	110.1	0.9	0.824
Average Value	108.5	109.6	1.1	1.014

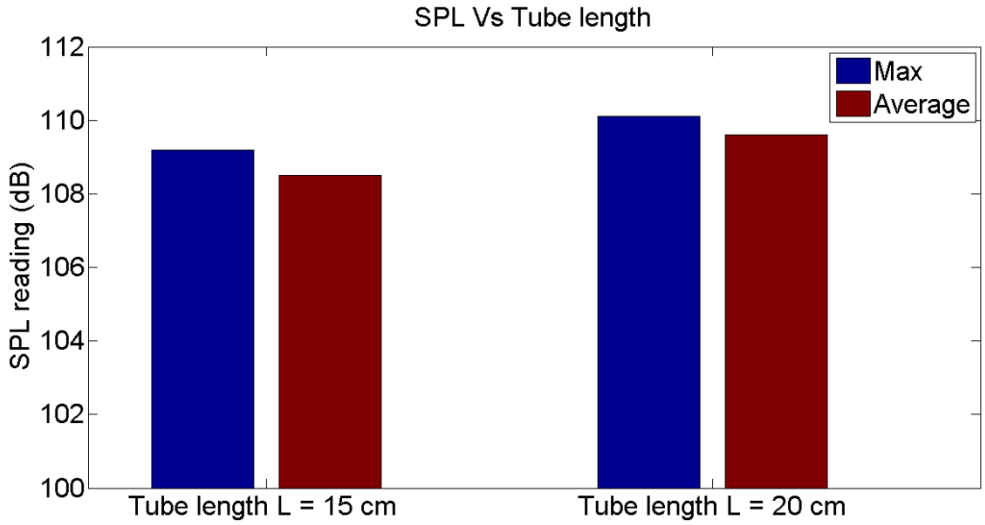

Figure 4.9: SPL (max and average) vs tube length for stack length l = 2.5 cm

4.5 SPL vs Input Power

The effect of input power on output sound pressure level was also observed. Input power was varied by varying the voltage drop across the Nichrome wire. Variable resistance was used for this purpose. A 15 cm long laser was used for this test. Increasing the input voltage generated higher sound pressure levels. Higher input voltage generates a higher temperature gradient across the stack, which in turn produces higher acoustic power output. This is evident from equation 4.3, according to which the power output is proportional to the ratio $= \nabla T_m / \nabla T_{crit}$. Results of the experiment are presented in Table 4.3 and in Figure 4.10.

To understand this phenomenon from a Lagrangian point of view, consider Figure 4.11 displaying the cycle of an acoustic prime mover. When the input voltage is

Table 4.3: Sound pressure level measurements for different input voltages (L is the length of the tube, l is the length of stack, d is distance of stack from the closed end, r is distance from tube opening and, V_{in} is input voltage)

Experimental Setup (l = 2.5 cm, r = 10 cm, d = 5 cm, L = 15 cm)	SPL reading (dB) for V_{in} = 6 V	SPL reading (dB) for V_{in} = 6.5 V	Rise in SPL reading (dB)	Percentage rise (%)
Max Value	107.7	109.2	1.5	1.4
Average Value	106	108.4	2.4	2.26

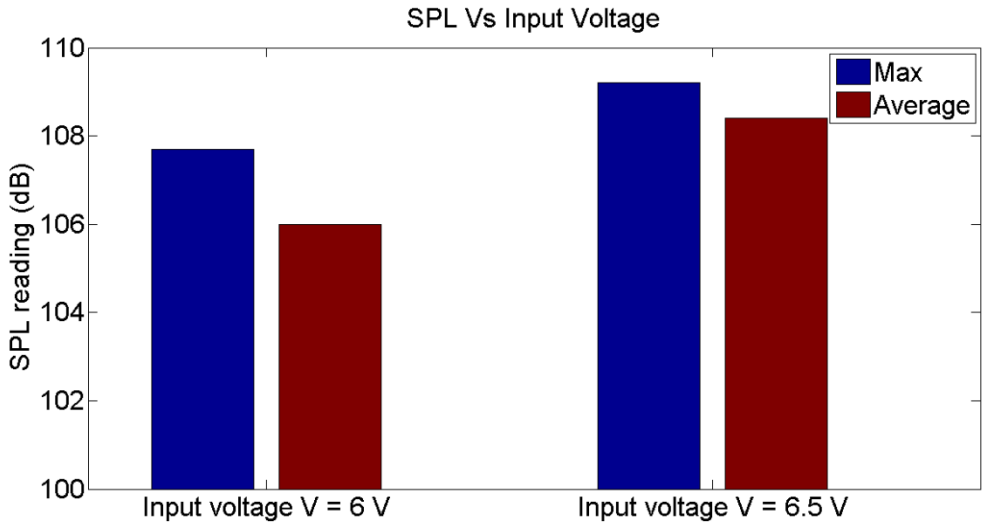

Figure 4.10: SPL (max and average) vs Input Voltage

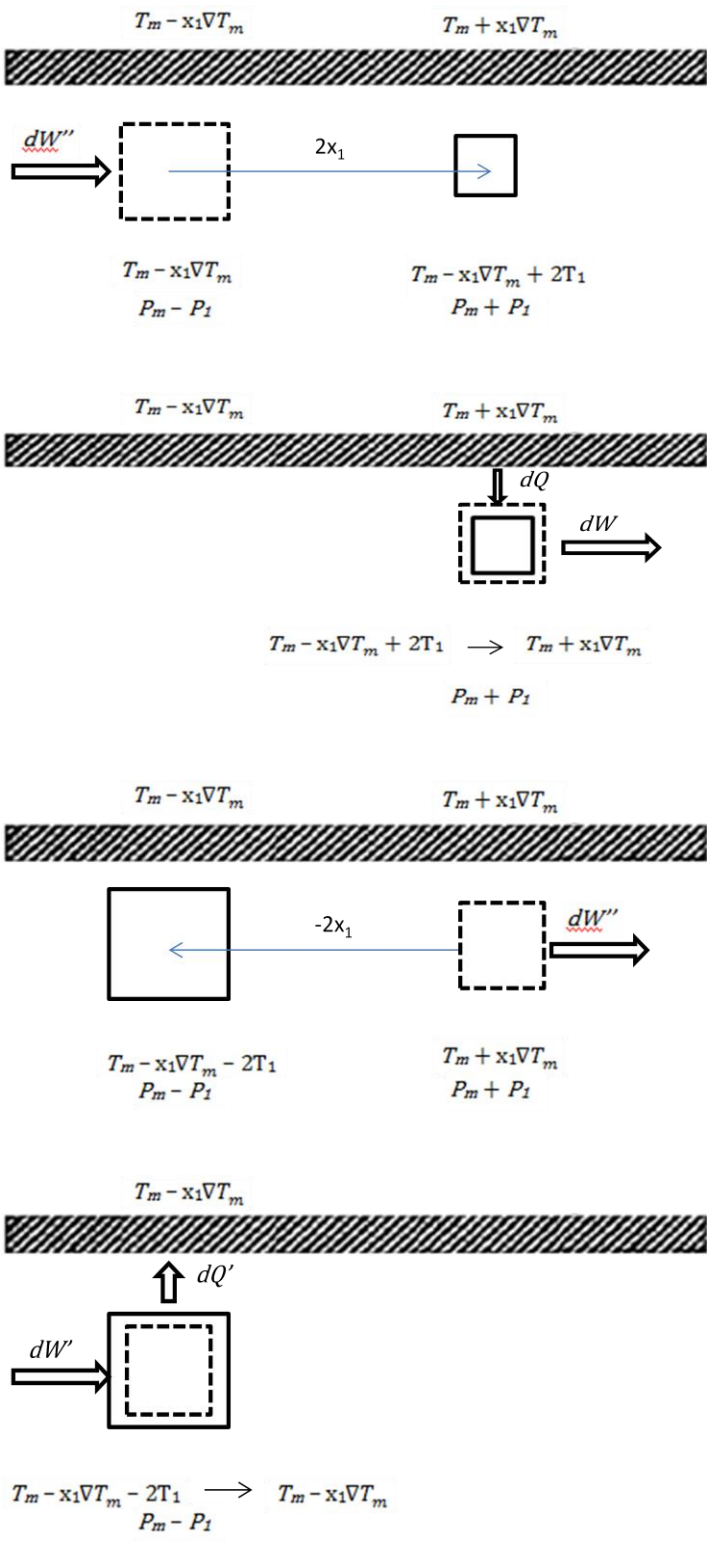

Figure 4.11: Cycle of an acoustic engine serving as a prime mover

increased, the temperature gradient across the stack increases. This results in higher heat transfer to and from the fluid parcel, which amplifies the output sound wave.

4.6 High-Frequency Thermoacoustics

High-frequency Thermoacoustic lasers can be constructed by reducing the length of the resonator. A comparison of two prime movers of lengths 10 cm and 20 cm is presented herein. The resonant frequency depends on the length of the prime mover. The fundamental resonant frequency is given by equation 4.1 and for quarter wavelength prime movers of length L, λ is given by equation 4.2.

A 2.5 cm long stack was used in both the Thermoacoustic lasers and it was positioned at a distance of L/4 from the closed end of the resonator. SPL readings and microphone readings were taken at 10 cm from the open end. The USB 2009 data acquisition device and SignalExpress were used to acquire and analyze the signal. The 10 cm long prime mover recorded the fundamental frequency of 885 Hz and the 20 cm long recorded 437 Hz, which are comparable to the theoretical values (860 Hz and 430 Hz) obtained by equations 4.1 and 4.2. Waveforms and frequency graphs for both the prime movers are compared in Figure 4.12, Figure 4.13, Figure 4.14, and Figure 4.15.

Sound pressure level (SPL) is a logarithmic measure of the effective sound pressure of a sound relative to a reference value. It is measured in decibels (dB) above a standard reference level and is given by:

$$SPL = 20log_{10}(\frac{P_{rms}}{P_{ref}}) \qquad (4.3)$$

where P_{rms} is the rms sound pressure being measured and P_{ref} is the reference sound pressure. A commonly used P_{ref} value is 20 μPa (rms).

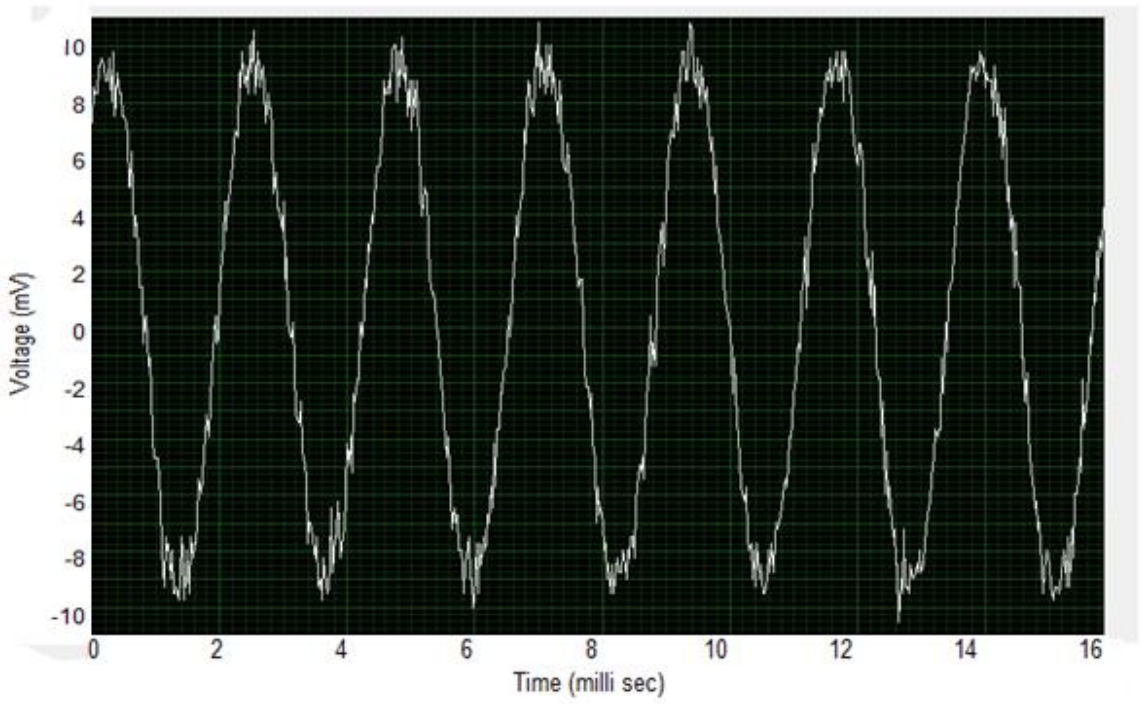

Figure 4.12: Signal generated by 20 cm long Thermoacoustic laser

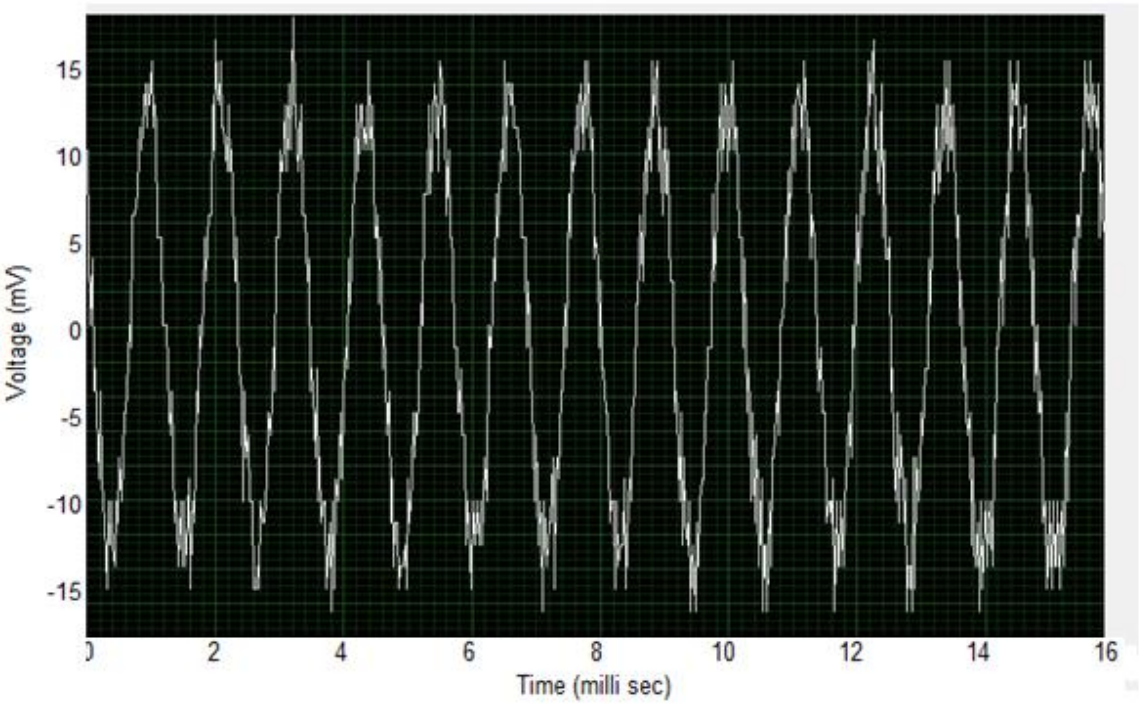

Figure 4.13: Signal generated by 10 cm long Thermoacoustic laser

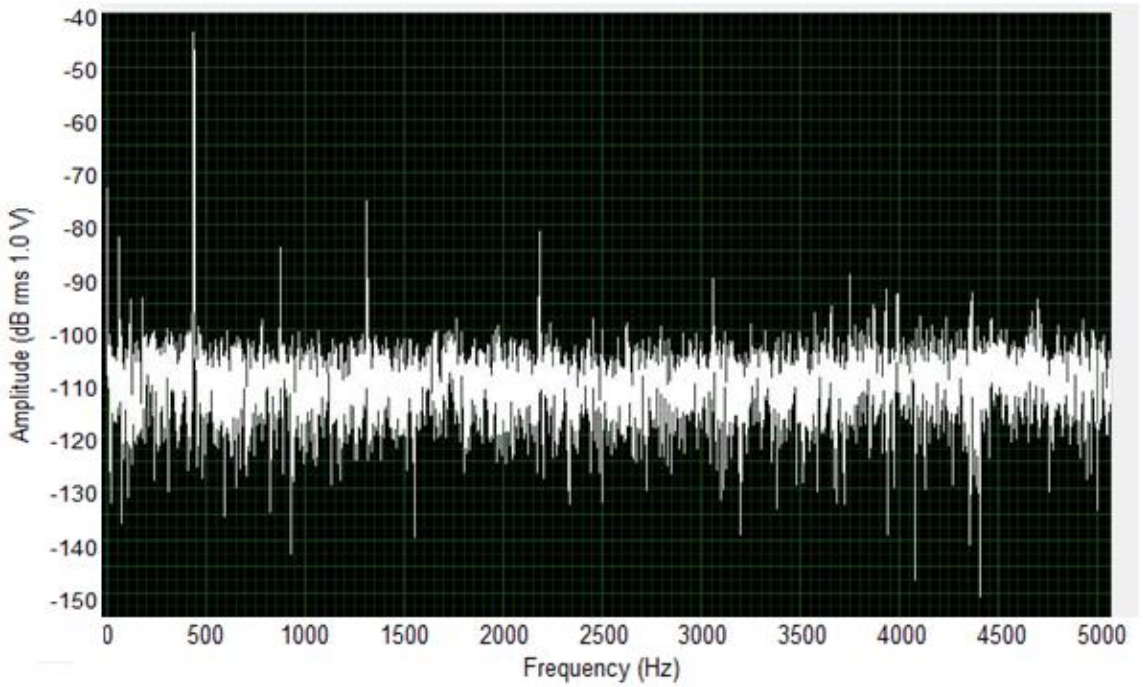

Figure 4.14: Frequency chart for a 20 cm long Thermoacoustic laser

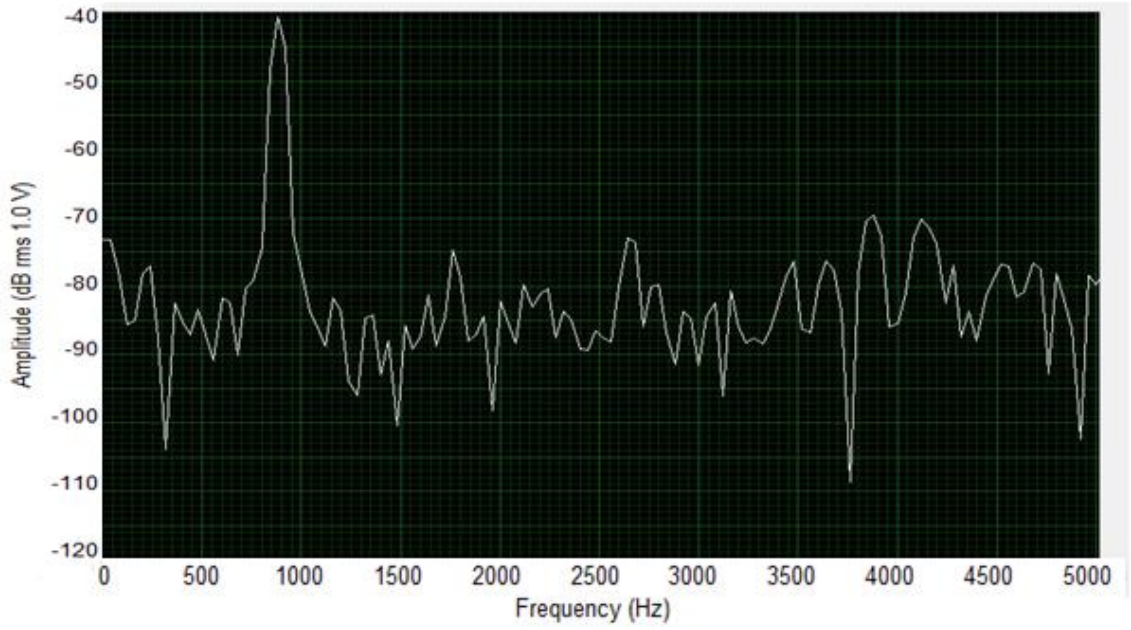

Figure 4.15: Frequency chart for a 10 cm long Thermoacoustic laser

For the 20 cm long Thermoacoustic laser, the SPL reading at a distance of 10 cm from the tube opening and along the axis of the tube was 106.3 dB. Using equation 4.4, the P_{rms} value obtained for the 20 cm long Thermoacoustic laser was 4.13 Pa. V_{rms} generated by the microphone and recorded by the Amplitude and Level step of SignalExpress was 6.71 mV. Thus, the gain of the microphone was V_{rms}/P_{rms} = 1.62 mV/Pa.

For the 10 cm long Thermoacoustic laser, the SPL reading at a distance of 10 cm along the axis of the tube from the tube opening was 109.4 dB. Using equation 4.4, P_{rms} value obtained for the 10 cm long prime mover was 5.90 Pa. V_{rms} generated by the microphone and recorded by the Amplitude and Level step of SignalExpress was 9.63 mV. Thus, gain of the microphone was V_{rms}/P_{rms}= 1.63 mV/Pa.

The sound generated by the 10 cm long Thermoacoustic laser with a 1.25 cm long stack reached its maximum value quickly and then suddenly dropped down to zero. Stacks of length 25 cm and 12.5 cm were tested. The 25 cm long stack did not generate any sound at all. Shorter Thermoacoustic lasers of lengths 2.5 cm, 5 cm, and 7.5 cm were also tested for generating high-frequency outputs. 1 cm and 1.5 cm long stacks were used in these prime movers. None of these Thermoacoustic lasers could produce sound. One possible explanation of this phenomenon could be the insufficient temperature gradient generated in this prime mover. Young Sang Kwon (2006) studied high-frequency Thermoacoustic Prime Movers operating at frequencies between 2 KHz and 25 KHz and observed that a large temperature gradient was needed to produce sound. For a given temperature difference and given wavelength of the prime mover, the maximum stack length to set up oscillations is given by:

$$\nabla x_{max} \approx \frac{\lambda \nabla T}{T_m \tan\left(\frac{x}{\lambda}\right)} \quad (4.4)$$

where λ is the wavelength of the prime mover and ∇T is the temperature difference between the two ends of the stack. Young Sang Kwon (2006) observed that the prime movers could work only when the stack length ∇x is less than ∇x_{max} for the given wavelength of the prime mover and given temperature difference across the stack.

4.7 Acoustic Power Output of a Thermoacoustic Laser

A Thermoacoustic laser radiates acoustic power which results in sound pressure oscillations. Sound pressure is relatively easier to measure using an SPL meter. Using equation 4.3, an rms value of pressure oscillations can be calculated. Sound pressure oscillations on the eardrum which we perceive as sound are the same pressure oscillations which are detected by the condenser microphone of a SPL meter. The sound pressure reading measured by a SPL meter depends on distance from the source and the acoustic environment in which the sound waves are present. This in turn depends on the size of the room and the sound absorption of the surfaces. Thus, measuring the sound pressure cannot necessarily quantify the sound power radiated by a Thermoacoustic laser. However, the radiated sound power can be estimated by taking the product of the sound intensity and the surface area of the spherical wave at a point far away from the tube opening (Garrett 2005; Matveev et al. 2008). At a point far away from the tube opening, the effects of the reflected sound wave from the surface of the SPL meter are reduced. Thus, the estimated radiated power is given by:

$$P_{out} = 4\pi r^2 P_{rms}{}^2/(\rho_0 C) \quad (4.5)$$

where r is the distance from tube opening, P_{rms} is the rms value of pressure fluctuations, ρ_0 is density of the air and, C is the speed of sound.

Garrett (2005) suggested that the sound pressure measurement recorded at 1 meter from the tube opening provides a useful (not exact) measurement of the total radiated acoustic power. Experiments were conducted to measure the SPL readings at different distances from the tube opening and along the axis of the tube. The corresponding sound power outputs were calculated using equation 4.5. The results are as shown in Table 4.4.

For different locations from the tube opening, the acoustic power output varied from 17.23 mW to 27.32 mW. For a spherical wave, the acoustic power measured at any location from the point source should be the same. However, in our experiments, the acoustic power was calculated from the SPL reading, which depends on the room size and sound absorption of the surfaces.

Sound power can be accurately measured by measuring both pressure and particle velocity. Sound intensity is the time-averaged product of pressure and particle velocity. Pressure can be calculated by knowing the SPL reading and using the equation 4.3, but measuring particle velocity is not simple. The particle velocity, however, can be related to the pressure gradient (the rate at which the instantaneous pressure changes with

Table 4.4: Sound power calculated at different distances from the tube opening

Distance from the tube opening (m)	SPL (dB)	Prms (Pa)	Power (mW)
0.25	104.2	3.24	23.56
0.5	97.4	1.48	19.69
0.75	95.3	1.16	27.32
1	90.8	0.69	17.23
1.25	89.4	0.59	19.50

distance) with the linearized Euler equation. With this equation, it is possible to measure this pressure gradient with two closely spaced microphones and relate it to particle velocity. Sound intensity can also be accurately measured by commercially available sound intensity meters.

4.8 Uncertainty Analysis

In order to provide the reader with some measure of the reliability of the results of the experiments, uncertainty analysis was done based on the methods described by Kline and McClintok (1953). Uncertainty is the possible value an error might have. All the uncertainty estimates were based on 95 percent confidence levels. The uncertainty interval for voltage measured by the multimeter was w_V = ± 0.25 V as specified by the manufacturer. NiCr wire resistances were calculated by measuring the length of the wire and then multiplying this number by the specific resistance of NiCr wire. Specific resistance of 26 gauge Nichrome (NiCr) resistance heater wire is 2.571 Ohm/ft, as specified by the manufacturer. The uncertainty interval of length measurements was assumed to be ± 0.002 m, which gave the uncertainty interval for resistance measurements as w_R = 0.002*2.571/0.3 = 0.01714 Ohm. The uncertainty interval of the sound pressure level measurement was 1.5 dB, as specified by the manufacturer. The uncertainty interval in Power was determined by using the theorem stated in the paper by Kline and McClintok (1953). According to the authors, if R is the linear function of n independent variables, each of which is normally distributed, then the relation between the interval for the variables w_i, and the interval for the result is:

$$w_R = \left[\left(\frac{\partial R}{\partial v_1} w_1\right)^2 + \left(\frac{\partial R}{\partial v_2} w_2\right)^2 + \ldots\ldots + \left(\frac{\partial R}{\partial v_n} w_n\right)^2\right]^{1/2} \qquad (4.6)$$

Power was calculated by using equation 3.1. Based on equations 3.1 and equation 4.6, the uncertainty interval for power is given by:

$$w_p = [\left(\frac{\partial P}{\partial V} w_V\right)^2 + \left(\frac{\partial P}{\partial R} w_R\right)^2]^{1/2} \quad (4.7)$$

Using this equation, Power uncertainty was $\pm$ 11.45 % to $\pm$ 8.23 % for the range of power values from P = 18.94 W to P = 37.44 W.

Theoretical values of frequencies were calculated using the equation $f_o = a/4L$ where a is the speed of sound. Using this equation, the uncertainty interval for the frequency is given by:

$$w_f = \frac{\partial f}{\partial L} w_L \quad (4.8)$$

Using this equation, the uncertainty in the frequency measurement was $\pm$ 1 % to $\pm$ 2 % for f_o= 430 Hz to f_o = 860 Hz.

CHAPTER 5

CONCLUSIONS

The research presented in this thesis dealt with the effects of geometric parameters of a Thermoacoustic laser on the output sound wave. Shorter prime movers were also tested to obtain high-frequency sound waves. In particular, geometric factors including the stack position, stack length, and tube length and the input voltage were varied. The experimental results were presented and were interpreted either qualitatively or quantitatively. The SPL measurements in the different orientations (0^o, 45^o, and 90^o) did not differ significantly, which confirms that the sound wave generated could be assumed to be a spherical wave. Three stacks of lengths 1.25 cm, 2.5 cm, and 5 cm were used in this study. Experiments were repeated for two different lengths of the resonator: 15 cm and 20 cm. It was observed that the maximum sound pressure level was generated for the laser with the stack positioned at a distance of L/4 lengths from the closed end of the resonator. Results were consistent across all the sets of experiments. The effects of stack position on the output sound pressure level were also observed. 1.25 cm, 2.5 cm, and 5 cm long stacks were tested in two prime movers of lengths 15 cm and 20 cm. For the experimental conditions studied in this research, the sound pressure levels increased with the increasing lengths and the 5 cm long stack recorded the maximum sound pressure level in both the prime movers.

The Thermoacoustic laser with 20 cm long resonator recorded more sound pressure level than the one with 15 cm long resonator when the same stack was used keeping the same input voltage. Higher input voltage generated higher temperature difference across the stack. This increased the heat transfer to and from the parcel of the fluid in a standing wave, thus amplifying the sound wave. A 10 cm long Thermoacoustic laser made from Pyrex generated sound wave of frequency 885 Hz whereas a 20 cm long prime mover of the same material generated 437 Hz sound wave. The shorter Thermoacoustic lasers did not generate sound power. A potential reason could be the insufficient temperature gradient across the stack. The maximum acoustic power recorded by the acoustic lasers studied in this research was 20.24 mW for 39 W of electrical input power.

The primary limitation with conducting the current experiments was the inability to try different materials for the resonator, stack, and heat exchangers. In particular, considerable amounts of heat losses were observed from the resonator body to the environment, which resulted in lower efficiencies of the Thermoacoustic lasers studied here. Stacks with different material, plate spacing, and thickness were not tested due to the difficulties involved with their manufacturing. Temperature measurement across the stack was not possible since there is a difference in temperature between the heating element and the hot end of the stack. Also, the temperature distribution across the stack is not linear (Wheatley et al. 1984), which further complicates the temperature measurements across the stack. However, our experimental findings compared well with the findings reported by other studies and were consistent with the previous theoretical studies.

Further work is needed to improve the efficiency and to produce high-frequency acoustic output by trying different materials for resonators, stack, and heat exchangers. Different stack geometries need to be studied for producing higher acoustic output. Experimental findings of this study helped us better understand the effects of geometric parameters on the output of the prime mover. Consequently, there are several important factors for amplifying the output intensity of a Thermoacoustic laser. Increasing the stack surface area by increasing the length of the stack creates higher output. However, in higher frequency Thermoacoustic Prime Movers, this is not a feasible option since the overall length of the prime mover is less for higher frequency devices. Positioning of the stack within the resonator is also important; our investigation suggests that the optimum position is at a quarter of the length of the Thermoacoustic laser from the closed end of the tube. Material of the tube is also an important factor for operating a Thermoacoustic laser. It is recommended that good conducting materials be tested for making the body of the resonator. This will enhance the heat transfer to and from the ends of the stack, which might further improve the performance of these devices. Applications of the Thermoacoustic Prime Movers were also discussed in this study. Thermoacoustic Prime Movers do not require moving parts or environmentally harmful working fluids. Simplicity of operation and high efficiency of Thermoacoustic devices could open new faucets for environmentally friendly options to industries as diverse as medical applications, natural-gas liquefaction, refrigeration, and air conditioning.

APPENDIX

Table A.1: Specifications of CEN-TECH 98025 multimeter

Power Requirements	9V Battery
Frequency	45 to 450 Hz
DC Amps	Range: 200mA/2000mA/20mA/ 10A
Accuracy	(@0mA-200mA) 1.2%±2D; (@10A) 3%±2D
DC Voltage	Ranges: 200mV/2000mV 20/200/1000V
Accuracy	(@200mV) 0.5%±1D (@2000mV-200V) 1%±2D (@1000V) 1%±2D
Resistance	Ranges: 200/2000/20K/200K/2000K Ohm

Table A.2: Specifications of Tenma 72-942 sound level meter

Standard applied	IEC651 type 2, ANSI S1.4 type 2
Frequency range	31.5Hz to 8kHz
Measuring level range	30 to 130dB
Frequency weighting	A/C
Microphone	½ inch electret condenser microphone
Display	LCD
Resolution	0.1 dB
Display Up data	0.5 sec
Time weighting	FAST(125mS), SLOW(1 sec.)
Level ranges	Lo: 30-100dB Hi: 60-130dB
Accuracy	± 1.5dB (under reference conditions)
Maximum hold	Hold readings the Maximum Value, with decay < 1dB/3minutes
Operation temperature	0 to 40°C (32 to 104°F)
Operation humidity	10 to 90%RH
Dimensions	201(L) x 55(W) x 32(H) mm
Weight	230g (including battery)

Table A.3: Specifications of NI USB 6009

Feature	**NI USB-6009**
AI Resolution	14 bits differential, 13 bits single ended
Maximum AI Sample Rate, Single Channel*	48kS/s
Maximum AI Sample Rate, Multiple Channels (Aggregate)*	48kS/s
DIO Configuration	Open Collector or Active Drive
* System Dependant	

Table A.4: Analog terminal assignments for NI USB 6009

Terminal Signal	Single-Ended Mode Signal	Differential Mode
1	GND	GND
2	AI 0	AI 0+
3	AI 4	AI 0-
4	GND	GND
5	AI 1	AI 1+
6	AI 5	AI 1-
7	GND	GND
8	AI 2	AI 2+
9	AI 6	AI 2-
10	GND	GND
11	AI 3	AI 3+
12	AI 7	AI 3-
13	GND	GND
14	AO 0	AO 0
15	AO 1	AO 1
16	GND	GND

REFERENCES

Bisio, G., Rubatto, G., 1999. Sondhauss and Rijke oscillations—thermodynamic analysis, possible applications and analogies. Energy 24(2), 117-131.

Ceperley, P. H., 1979. A pistonless Stirling engine–The traveling wave heat engine. Journal of Acoustical Society of America 66, 1508-1513.

Fahey, D., 1992. Thermoacoustic oscillations in cryogenics. Part 3: avoiding and damping of oscillations. Cryogenics 32(8), 703-706.

Feldman Jr, K.T., 1968. Review of the literature on Sondhauss thermoacoustic phenomena. Journal of Sound and Vibration 7(1), 71-82.

Feldman Jr, K.T., 1966. A study of heat generated pressure oscillations in a closed end pipe. PhD. thesis, University of Missouri.

Garrett, S. L., Backhaus, S., 2000. The Power of Sound. Sigma Xi, The Scientific Research Society 88(6), 516-525.

Garrett, S. L., 2005. Acoustic laser kit instructions. Applied Research Laboratory, Penn State University, State College, PA.

Huelsz, G., Ramos, E., 1996. A physical interpretation of the thermoacoustic effect. Journal of Non-Equilibrium Thermodynamics 21(3), 278-284

Huelsz, G., Ramos, E., 1999. An experimental verification of Rayleigh's interpretation of the Sondhauss tube. The Journal of the Acoustical Society of America 106(4), 1789.

Kim, Y.T., Kim, M.G., 2000. Optimum positions of a stack in a thermoacoustic heat pump. Journal of the Korean Physical Society 36(5), 279-286.

Kline, S. J., McClintock, F. A., 1953. Describing uncertainties in single-sample experiments. Journal of Mechanical Engineering 75, 3-8.

Kwon, Y. S., 1996. Study of Thermoacoustic engines operating at frequencies between 2 KHz and 25 KHz. PhD thesis, The University of Utah.

Lampe, R., 2008. Design and testing of rapid prototyped stacks for thermoacoustic applications. In Proceedings of The National Conference On Undergraduate Research (NCUR).

Matveev, K. I., Shafiei-Tehrany N, Richards, C. D., 2008. Small-scale thermoacoustic engine demonstrator. In Proceedings of PowerMEMS 2008 + microEMS, Dendai, Japan.

Rayleigh. (a.k.a John William Strutt) 1878. The explanation of certain acoustical phenomena. Nature (London) 18, 319-321

Rott, N., 1980. Thermoacoustics. Advances in Applied Mechanics 20, 135-175

Swift, G., 1988. Thermoacoustic Engines. The Journal of the Acoustical Society of America 84, 1145-1180

Swift, G., 2004. What is thermoacoustics?. Condensed Matter and Thermal Physics Group, Los Alamos National Laboratory, 1-6

Symko, O., 2004. Design and development of high-frequency thermoacoustic engines for thermal management in microelectronics. Microelectronics Journal 35(2), 185-191.

Symko, O.G., 2010. Acoustic approach to thermal management: miniature Thermoacoustic engines. In Thermal and Thermomechanical Proceedings 10th Intersociety Conference on Phenomena in Electronics Systems, 2006, 771-776.

Tijani, M.E.H., Zeegers, J.C.H., de Waele, a. T. a. M., 2002. The optimal stack spacing for thermoacoustic refrigeration. The Journal of the Acoustical Society of America 112(1), 128.

W. C. Ward and G. W. Swift, 1994. Design environment for low-amplitude thermoacoustic engines. The Journal of the Acoustical Society of America 95, 3671–3672

Waxler, R., 2001. Stationary velocity and pressure gradients in a thermoacoustic stack. The Journal of the Acoustical Society of America 109(6), 2739.

Wheatley, J., Hofler, T. & Migliori, A., 1983. An intrinsically irreversible Thermoacoustic heat engine. The Journal of the Acoustical Society of America 74(1), 153-170